FINAL TECHNICAL REPORT

OWRRI PROJECT DETERMINATION OF FRACTURE DENSITY IN THE ARBUCKLE-SIMPSON AQUIFER FROM GROUND PENETRATING RADAR (GPR) AND RESISTIVITY DATA

AUGUST 2008

Prepared for:

Oklahoma Water Resources Research Institute
003 Life Sciences East, OSU
Stillwater, Oklahoma 74078-3011

Prepared by:

Ibrahim Cemen
OSU School of Geology
105 Noble Research Ctr
Stillwater, OK 74078

Roger Young
University of Oklahoma
School of Geology and Geophysics
100 East Boyd St. Ste 810
Norman, OK 73019

Todd Halihan
OSU School of Geology
105 Noble Research Ctr
Stillwater, OK 74078

Table of Contents

Report

Appendices

1.0 Introduction

The ground water resources of Oklahoma are vital to the economic well being of the state. In order to properly manage these resources, an understanding of the discharge and recharge of aquifers is necessary. Fractures in aquifer rocks affect the flow of water. Therefore, numerical modeling of the fluid flow requires an understanding of the geometry and density of fractures that have a great influence on the discharge and recharge mechanisms.

1.1 Project Objective

The Arbuckle-Simpson aquifer of southern Oklahoma is a major source of drinking water for communities in the south-central part of the state. In outcrops, the carbonate units of the Arbuckle-Simpson are highly fractured. The basement rocks underlying the Arbuckle-Simpson aquifer are also highly fractured in outcrop. However, the orientation and density of fractures are different in the basement than the Arbuckle-Simpson aquifer. For example, the granites exposed in the Devil's Den area near Tishomingo, Oklahoma exhibit extensive fracturing and faulting. The carbonates of the Arbuckle-Simpson aquifer in the Spear's ranch contain only fractures. Moreover, fracture densities are very different within the two areas. The characterization of fractures in the basement is also important for ground water modeling work currently underway at both the Oklahoma Water Resources Board (OWRB) and the United States Geological Survey (USGS). Therefore, mapping fracture density from geophysical data such as Ground Penetrating Radar (GPR), Electrical Resistivity Imaging (ERI), and seismic data would provide timely information for these modeling studies. When tied to outcrop fracture data, significant information can be obtained regarding the fracture properties of these formations.

1.2 Application of GPR Techniques in Fractured Rock Environments

Characterization of fracture systems in competent rocks by the GPR method is effective in evaporates and in crystalline basement rocks. Young and Ramirez (2007) show that electromagnetic ray paths that cross fractures in evaporates at different angles of incidence will travel at different velocities and this , then, gives a means of determining fracture orientation. Holloway et al. (1992) used both surface and borehole GPR to examine Precambrian granite of the Canadian Shield in order to rank sites for subsurface radioactive waste disposal in Manitoba. They found a correlation between reflections and large aperture, open fractures on the one hand and between reflection swarms and multiple small fractures on the other.

GPR wavefields penetrate to depths of several tens of meters in carbonates and granites but where there is attenuation due to higher conductivity lithologies, such as a soil mantle or heavily weathered epikarst, detection of geological targets is restricted to shallower depths . Lower frequency antennas maximize the depth of investigation, but at the same time, diminish resolution. Our antenna choice in the surveys of this project was 100 MHz unshielded antennas.

Processing flow

The first processing step increases the signal strength during recording. GPR waves travel at a large fraction of the speed of light and therefore take very little time to travel from the transmitter to the receiver. This permits vertical stacking of the GPR traces in real time, that is, the superposition of up to 1024 traces at each location during the survey thereby increasing the signal/noise ratio considerably.

Processing of raw GPR data is necessary to remove noise further and to enhance signal by restoring signal strength lost to spherical spreading and frequency-dependent attenuation (spherical and exponential correction). Artifacts of the recording process must also be removed (dewow). Unlike a seismic survey, the time at which the GPR trace begins is not the instant the transmitter fires. Removing this delay is termed time-zero correction. Finally, bandpass filtering also helps separate signal from noise.

Although stacking decreases *random* noise, spurious reflections and diffractions from metal objects clutter up the desired image of the subsurface. Due to the high dielectric contrast between air or soil and metal, these unwanted signals are often much stronger than the reflections from geological boundaries—stratigraphic and structural—being sought. Because such objects are time invariant, stacking is ineffective.

Coherent noise reduction

Young and Sun (1999) devised an effective method for removing locally recognized, coherent noise from a GPR section and named this process *the domain filter*. It has proven very effective in removing coherent noise events. The principle coherent noise at the A-S Ranch is due to a buried pipe. At both the A-S Ranch and Devil's Den very shallow stratigraphy and fractures, respectively, are obscured by a noise mode traveling directly through the air from transmitter to receiver. We remove both the pipe response and the air wave using the domain filter.

Velocity analysis

Velocities characterize lithology thereby helping to identify a geologic unit traversed by a GPR wave. Velocity is also important to convert recorded two-way reflection travel times to depth. Velocity can be determined by using the method of velocity semblance developed for seismic reflection analysis. Velocity can also be found by constructing the linear traveltime curve, T(X), for the wave traveling at the earth's surface directly through the ground from a source location to a receiver location.

1.3 Application of ERI techniques in fractured rock environments

Fractured and karstic aquifers have been described for many years, but few field techniques to adequately characterize these complex aquifers exist. Much of our understanding of the flow in these aquifers has been generated from field experiments using wells or outcrops. The lack of characterization data generally comes from the cost involved in drilling, completing, maintaining and sampling wells. This cost is higher in fracture and karstic aquifers due to the higher drilling costs and the heterogeneous flow fields typically require more data than are available from discrete sampling techniques which provide only limited 2- or 3-dimensional data.

To resolve these difficulties, data are required that allow areas or volumes of the subsurface to be examined, instead of solely relying on discrete sampling data. Most importantly, methods employed need to be economical when compared to alternative techniques.

Existing methods of characterizing these aquifers have relied on two detection and monitoring strategies. The first strategy involves discrete point sampling of fluids using wells, springs or multilevel piezometers whose data is integrated and interpreted. The second strategy uses indirect measurements through surface or borehole geophysical techniques.

The difficulty with point sampling techniques is that sufficient sampling can be expensive because of drilling costs, sampling time, sample analysis and data integration and interpretation time. Additionally, determining whether fractures or karst features exist between sampling locations using piezometers can be difficult to impossible to determine. This point sampling method can miss conduits not sampled by wells, or barriers to flow like vertical faults that are not sampled with a traditional piezometer monitoring grid.

A solution to some of these sampling problems in the vadose and phreatic zones is the utilization of electrical resistivity imaging (ERI) to provide more complete site data coverage. A temporary surface system for site evaluation can be used as an evaluation of a 2-D or 3-D portion of subsurface or cable can be installed in boreholes to image to deeper depths with higher resolution. Cables can be permanently installed in shallow trenches or in boreholes for long-term monitoring applications.

Electrical resistivity measurements have been used since the 1830's to interpret the geology of the earth (Van Nostrand and Cook, 1966). The technique introduces current into the ground and the potential field is measured. ERT (Electrical Resistance Tomography) is a method of obtaining resistivity measurements that determines the electrical conductivity of the ground using subsurface electrodes (Daily et al., 2004). In contrast, a multielectrode array uses electrodes only on the surface. Electrical Resistivity Imaging (ERI) is a general term used to indicate that a high resolution electrical resistivity technique is being used without naming each electrode configuration differently.

An electrical resistivity image is an inverted model of hundreds to thousands of four electrode resistivity measurements. A single electrical measurement does not yield significant information, similar to a single pixel on a digital photo. However, hundreds of measurements of a site can produce a 2-D or 3-D electrical image of the subsurface.

This technique is occasionally used for site characterization, but it can be inefficient, expensive, or worse, ambiguous (Ramirez et al., 1993).

In general, flow features (such as faults that conduct fluids) and higher porosity lithologies are indicated by low resistivity anomalies. Additionally, the hydraulic parameters of the formation may be estimated using electrical methods (Purvance and Andricevic, 2000a, b). The electrical data produced from this type of study may help characterize heterogeneity, fractures, and aquifer parameters (Herwanger et al., 2004; Niwas and de Lima, 2003).

2.0 Site Description

Two sites were evaluated as part of this study. They include the Arbuckle Simpson Ranch west of Connerville, OK and the Devil's Den site south of Reagan, OK. The first site is Arbuckle-Simpson Ranch in southern Oklahoma. Dolomite of the Lower Arbuckle Group in this area is extensively fractured in outcrops in this area. The second site is in the Devil's Den area of Tishomingo, Oklahoma where Precambrian age granite is exposed at the surface. These granites are about 1.35 to 1.4 billion years old and form much of the basement rocks of southern Oklahoma (Suneson, 1997). The granite is highly fractured in places and is an excellent site for our work because of the absence of conductive overburden which limits the depth of penetration of GPR signal and electrical current. The granitic environment does present a challenge for drilling holes to plant electrodes in the ground for electrical resistivity work.

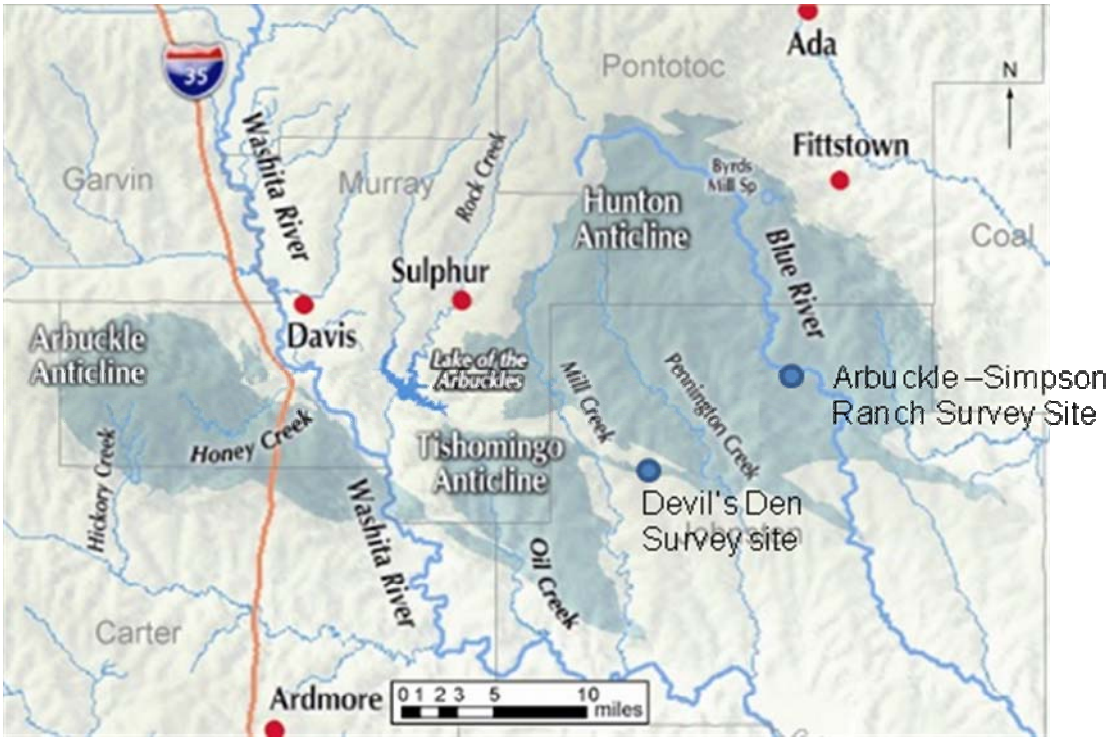

Figure 1: Map showing the locations of the Arbuckle-Simpson and Devil's Den sites surveyed during this investigation

.

3.0 GPR Data

3.1 GPR Data Collection

Description of pulseEKKO Pro 100 GPR system

Ground Penetrating Radar (GPR) measurements consist of recordings of an electromagnetic wave directed into the earth at a transmitter antenna and recorded at a receiver antenna. The downgoing wave is reflected from boundaries at which there is a change in dielectric permittivity. As with seismic waves, the greater the difference in permittivity across the boundary, the larger is the reflection coefficient and the stronger is the reflection recorded by the receiver antenna. Attenuation proportional to distance traveled (spherical spreading) and conversion of wave energy into heat (absorption) both diminish recorded reflection amplitudes. High electrical conductivity is the physical property most responsible for attenuation, and it is most often high conductivity that limits the depth to which GPR can see geological boundaries.

An EKKO Pro 100 system of Sensors and Software, Inc., recorded all GPR data acquired in the present project. Table 1 shows the survey and recording parameters for both sites at which data was acquired.

Arbuckle Simpson Ranch Survey

Line Name	Transmiter Voltage (Volts)	Source-Receiver Separation (m)	Station Spacing (m)	Record Length (ns)	Sample Interval (ns)	Vertical Stack Fold	Nominal Frequency (Hz)
GPR 1	400	1	0.5	200	0.8	64	100
GPR 2	400	1	0.5	200	0.8	64	100

Table 1a Survey and recording parameters at the A-S Ranch

Devil's Den Survey

Line Name	Transmiter Voltage (Volts)	Source-Receiver Separation (m)	Station Spacing (m)	Record Length (ns)	Sample Interval (ns)	Vertical Stack Fold	Nominal Frequency (Hz)
Line 1	400	1	0.5	200	0.8	64	100
Line 2	400	1	0.5	200	0.8	64	100
Line 3	400	1	0.5	200	0.8	64	100
Line 4	400	1	0.5	200	0.8	64	100
Line 5	400	1	0.5	200	0.8	64	100
Line 6	400	1	0.5	200	0.8	64	100
Line 7	400	1	0.5	200	0.8	64	100
Line 8	400	1	0.5	200	0.8	64	100
Line 9	400	1	0.5	200	0.8	64	100
Line 10	400	1	0.5	200	0.8	64	100
Line 11	400	1	0.5	200	0.8	64	100
Line 12	400	1	0.5	200	0.8	64	100
Line 13	400	1	0.5	200	0.8	64	100
Line 14	400	1	0.5	200	0.8	64	100
Line 15	400	1	0.5	200	0.8	64	100
Line 16	400	1	0.5	200	0.8	64	100
Line 17	400	1	0.5	200	0.8	64	100
Line 18	400	1	0.5	200	0.8	64	100
Line 19	400	1	0.5	200	0.8	64	100
Line 20	400	1	0.5	200	0.8	64	100
Line 21	400	1	0.5	200	0.8	64	100
Line 22	400	1	0.5	200	0.8	64	100
Line 23	400	1	0.5	200	0.8	64	100
Line 24	400	1	0.5	200	0.8	64	100
Line 25	400	1	0.5	200	0.8	64	100

Table 1b Survey and recording parameters at the Devil's Den

Survey sites

The present project recorded coincident GPR and ERI data at two geologically distinct locations, the Arbuckle-Simpson Ranch and Devil's Den (Figure 1). The A-S Ranch is on the south side of the Hunton Anticline. Here the geology is characterized by a relatively thick soil mantle overlying epikarst of the Arbuckle-Simpson Group. The GPR targets were the sub-horizontal boundaries between soil mantle and epikarst as well as the base of the epikarst seen in the resistivity profiles from the ERI surveys. In addition, we sought

to compare the ability of GPR to locate a sub-vertical boundary, namely, a fault detected by the ERI surveys of Halihan and coworkers and originally mapped by Ham (1964).

The Devil's Den area near Tishomingo, OK, lies south of the Hunton Anticline and is stratigraphically beneath the Arbuckle-Simpson Group(Figure 1). It consists of Precambrian granitic basement, which is highly faulted and fractured. The geological target at Devil's Den is the fractures as no lithologic layering is expected within the basement. Vertical fractures, on the other hand, can be seen clearly on the surface of the large outcrop over which we conducted the GPR measurements. We planned to assess the fracture density within the epikarst by GPR measurements and compare this to mapped fracture patterns obtained by Cemen (2008, personal communication) and co-workers.

3.2 GPR Data Reduction

The Arbuckle-Simpson Ranch 2D profiles

Our acquisition strategy at the A-S Ranch was to reoccupy the ERI lines surveyed by Halihan and students and to use GPR to image the same cross-sections of the subsurface in order to achieve a comparison between the two geophysical methods. This would establish whether the information from ERI and GPR is complementary in delineating horizontal contrasts in stratigraphy and in locating vertical discontinuities. Figure Y1 shows the line locations of all ERI and GPR profiles acquired at the A-S Ranch.

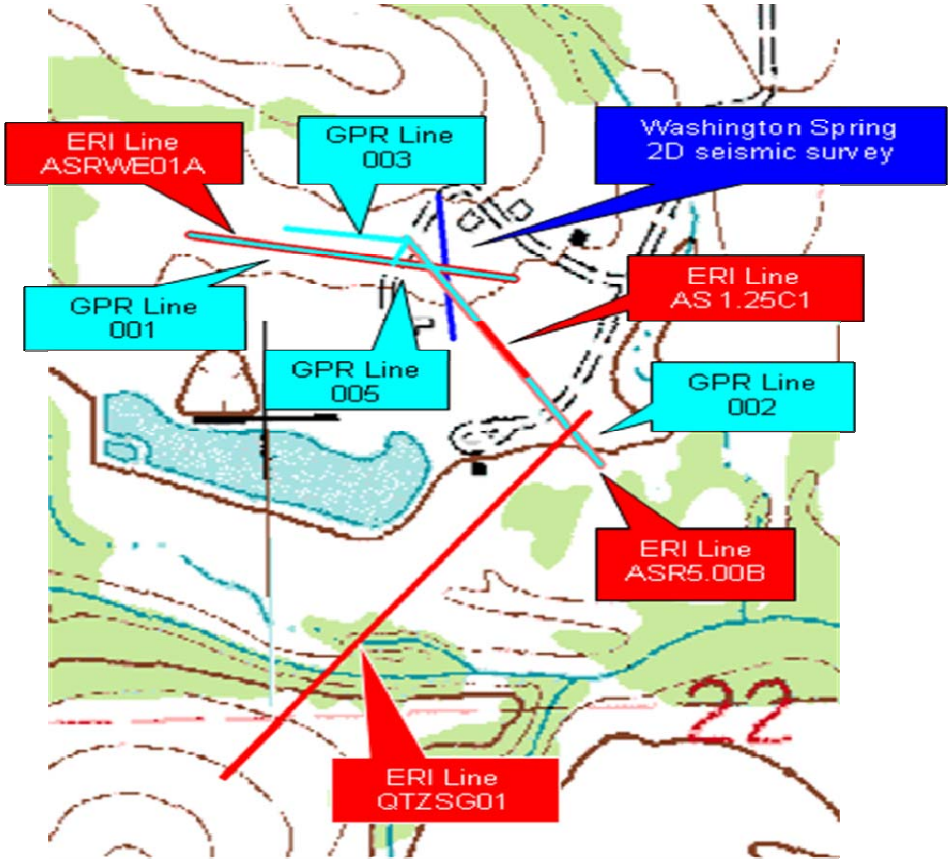

Figure 2: Map of all geophysical survey lines at the A-S Ranch

Processing flow

Processing of the A-S Ranch profiles is illustrated in Appendix A by a diagram showing how a segment of GPR Line 2 is changed by the different stages of processing. The final stage of processing (Figure A1e) shows that a 30 m long basinal feature exists at a time of 50-75 ns beneath the western half of the data segment. However, a coherent, westward dipping noise event still exists in the data (Figure A1e).

Another measure of success at noise reduction in processing is shown in Figure A2. After bandpass filtering, the frequency range in which signal occurs stands out more strongly from the frequency range of the noise.

Methods of coherent noise reduction

Appendix B shows the application of the domain filter to remove the dipping, non-geologic event left after processing (Figure B1a). This event is interpreted to be noise, possibly due to a reflection from a buried pipe. Before processing (Figure B1a), the

event overprints reflections of geologic significance. By transforming the selected event to the FK domain (Figure B2a), transforming it back to the X-T domain (Figure B2b) and subtracting it from the original data, the dipping event is removed. Figure B3 shows that after subtraction, a stratigraphic sag is now apparent.

Methods of velocity analysis

Auxiliary GPR surveys consisting of CMP gathers of traces were collected at the A-S Ranch in order to perform velocity semblance analysis. Two of these velocity analyses along GPR Line 2 are shown in Appendix C. Results for 8 CMP locations are shown in Table Y2. The average RMS velocity corresponding to a time of approximately 50 ns is .16 m/ns. Because most of the reflection raypath is in the uppermost epikarst-- and not in the much slower soil mantle-- this velocity for a carbonate rock should be consistent with the generally cited value of .12 m/ns (Annan, 2005). Our result is appreciably higher, but the difference may be that the Annan figure is for carbonates with appreciable porosity. The corresponding depth to the reflecting boundary within the epikarst is approximately 3.7 m. Figure C2 is a plot of the direct ground wave traveling through the soil mantle. The average velocity from two CMP gathers is approximately .05 m/ns

CMP Location	**Time (ns)**	**Velocity (m/ns)**
1	**58**	**0.16**
2	**47**	**0.16**
3	**60**	**0.17**
4	**N/A**	**N/A**
5	**57**	**0.17**
6	**60**	**0.15**
7	**61**	**0.15**
8	**N/A**	**N/A**
9	**43**	**0.18**
9	**54**	**0.15**
	Average Velocity	**0.16**

Table 2: RMS velocity at all A-S Ranch CMP locations

Devil's Den 3D survey

The GPR data at Devil's Den was acquired on an area of granite outcrop bearing no soil cover. Figure 3 shows the 25 parallel lines, each 100 m long, constituting the 3D survey The absence of soil cover hindered transmission of low frequency current into the ground for the ERI survey, but a coupling problem did not exist for transmission of GPR waves.

Processing flow

Processing of data at Devil's Den followed the same steps as at the A-S Ranch: dewow application, spherical and exponential correction, time-zero correction, and bandpass filtering (Appendix D). Figure D1e shows the presence of sub-horizontal reflections most likely due to variations in mineral banding within the granite. Bandpass filtering reloves both high and low frequency noise components.

There are also many steeply dipping events corresponding to diffractions from fractures in the granite. Migration will be applied to collapse these events back to the location of the fractures.

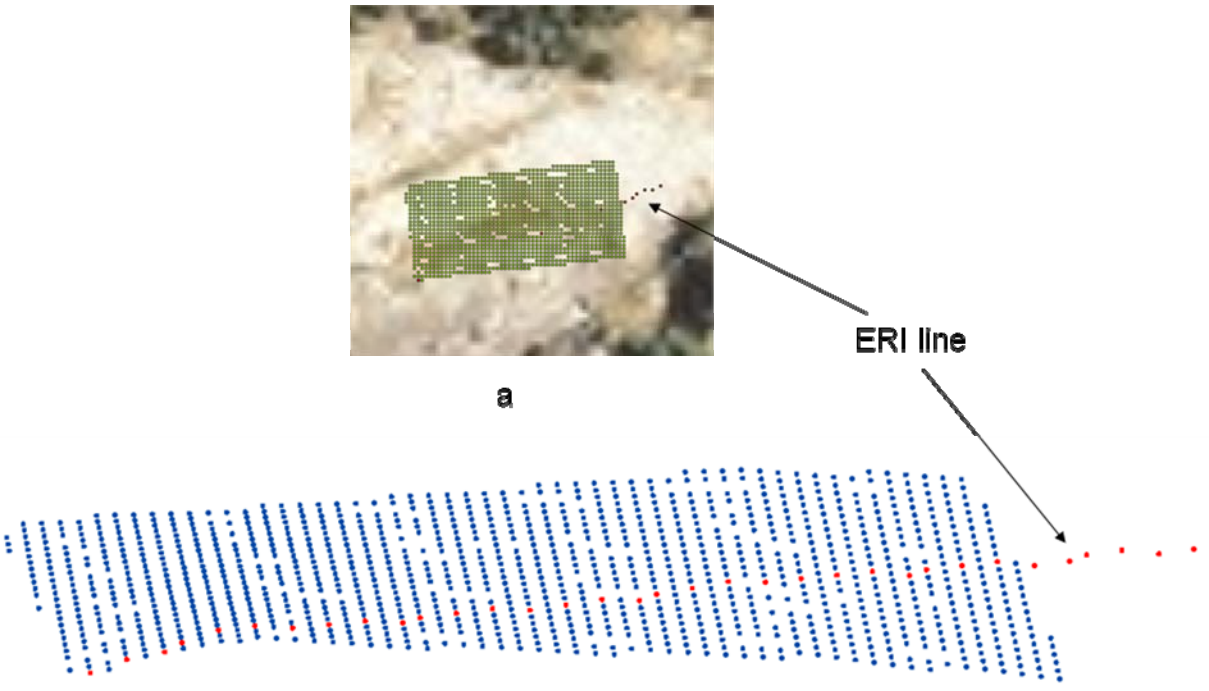

Figure 3: 3D GPR survey grid at Devils Den

Coherent noise reduction

The domain filter is used (Appendix E) to remove the airwave seen in Figure D1e so that very shallow underlying fractures can be seen. After filtering, diffractions from very shallow fractures (red circles, Figure E3b) extend the fracture imaging into an area formerly obscured by the airwave.

Velocity analysis

Because coherent reflections are absent from the data collected in the granite, the direct ground wave must be used to find the velocity of the granite. Figure F1 shows that velocities of the granite vary but are approximately .11 m/ns. This is somewhat lower than the average figure of .13 m/ns given by Annan (2005. We suspect that the occurrence of felsic dikes and extensive fracturing may play a role in determining the bulk velocity at this outcrop. Because we have chosen to profile across, rather than along, the predominant direction of fracturing, we would expect slower velocities as the GPR waves are impeded by these obstructions. Measurement made at many antenna orientations for each station have been successful in defining this velocity anisotropy in evaporates (Young and Ramirez, 2008) and this verification could be tried at Devil's Den.

3.3 GPR Data Interpretation

Principles of GPR interpretation

Both ERI and GPR measurements made on the ground's surface are indirect indicators of the underlying stratigraphy and degree of fluid saturation. Ground truth is absolutely necessary in order to pin a geological or lithological identity on either a resistivity boundary or a permittivity boundary.

At the A-S Ranch, Geoprobe cores and logs of a closely spaced sequence of five boreholes (Sample, 2008) provide shallow control, but no deeper ground truth is available. At Devil's Den, no ground truth is available. Due to this paucity of control, this report, for the most part, can point out correspondence of geophysical anomalies to mapped features but cannot confirm it. *Figure 4a shows location of Interpreted GPR section at A-S Ranch*

Interpretation of GPR Line 2 at the A-S Ranch

The purpose of the following section is to present one entire GPR line from the A-S Ranch and its interpretation. (Interpretation of the Devil's Den data is in Chapter 5 *Geophysical and Geological Data Integration.)*

Figure 4a: Showing the location of Interpreted GPR section at A-S Ranch

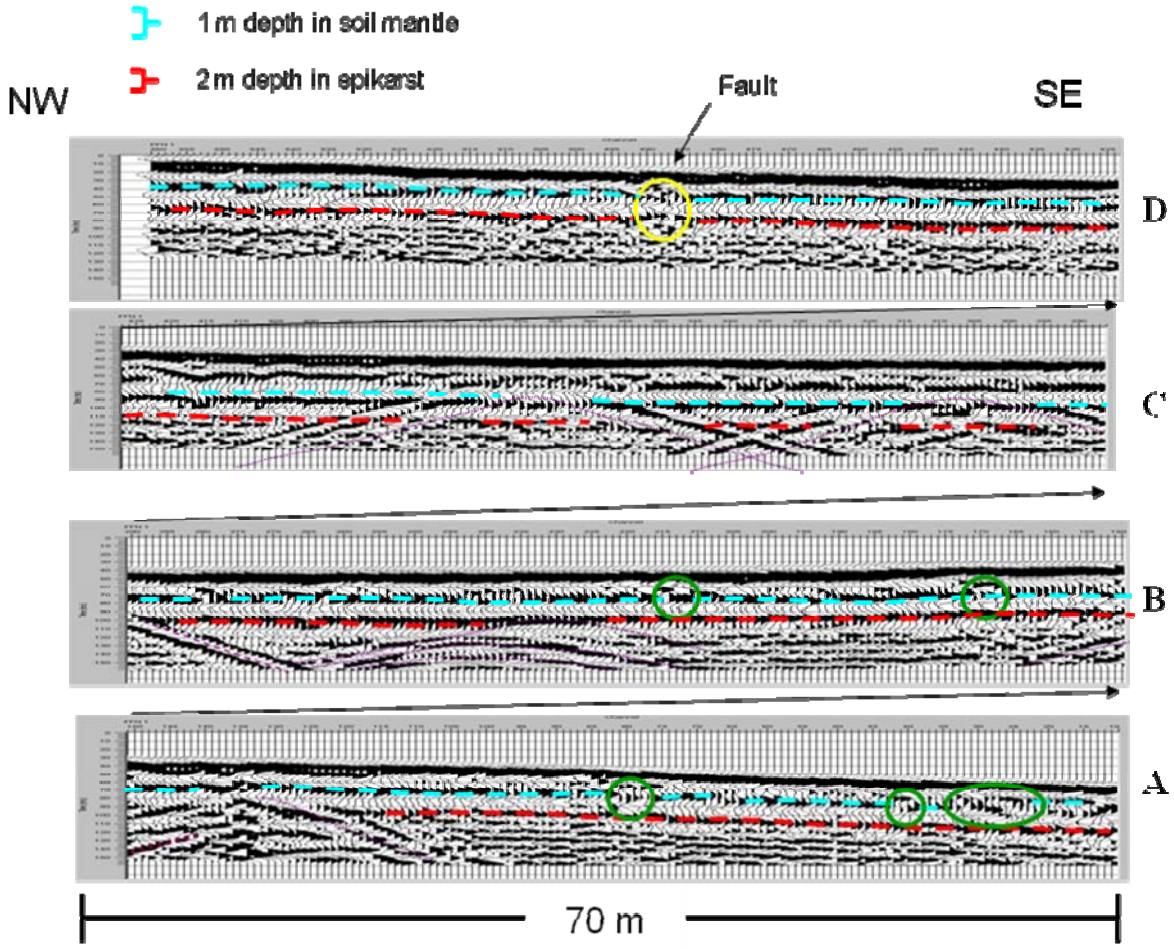

Figure 4b: Interpreted GPR section at A-S Ranch

Figure 4b consists of 560 GPR traces collected from SE to NW. In addition to the processing described in the appendices, the section has been topographically corrected. The line is spread out into four segments for detailed viewing. The vertical axis is in two-way time, but approximate conversion to depth is possible by using the scale bars at the top of the plot. Because velocity differs in soil and in epikarst, two scales are necessary.

Reflections from the base of the soil mantle(blue) and from a boundary within the epikarst (red) can be seen across the entire line. At places one or both boundaries are disrupted. The yellow circle shows disruption of both boundaries at a location corresponding to a mapped fault location (Todd Halihan, personal communication). Furthermore, it is in agreement with a fault (blue line, Figure 4b) seen on a near-surface seismic reflection survey (Kennedy and Young, in preparation) and on GPR line 1 where it intersects Line 2 (Figure 2). The green circles (Figure 4b) show shallow disruptions of the contact between the soil mantle and the epikarst. The large ellipse near the start of segment A indicates a portion of a basinal sedimentary feature where the soil mantle thickens.

The strong events (purple) cutting across segments A, B, and C are noise and are not of geological significance. Appendix B shows an example of how these features can be removed by further processing.

4.0 ERI Data

4.1 ERI Data Collection

An Advanced Geosciences, Inc. SuperSting R8 Earth Resistivity Meter (SuperSting) direct-coupled resistivity system was used to collect seven transects of ERI data at the study sites (Figure 5).

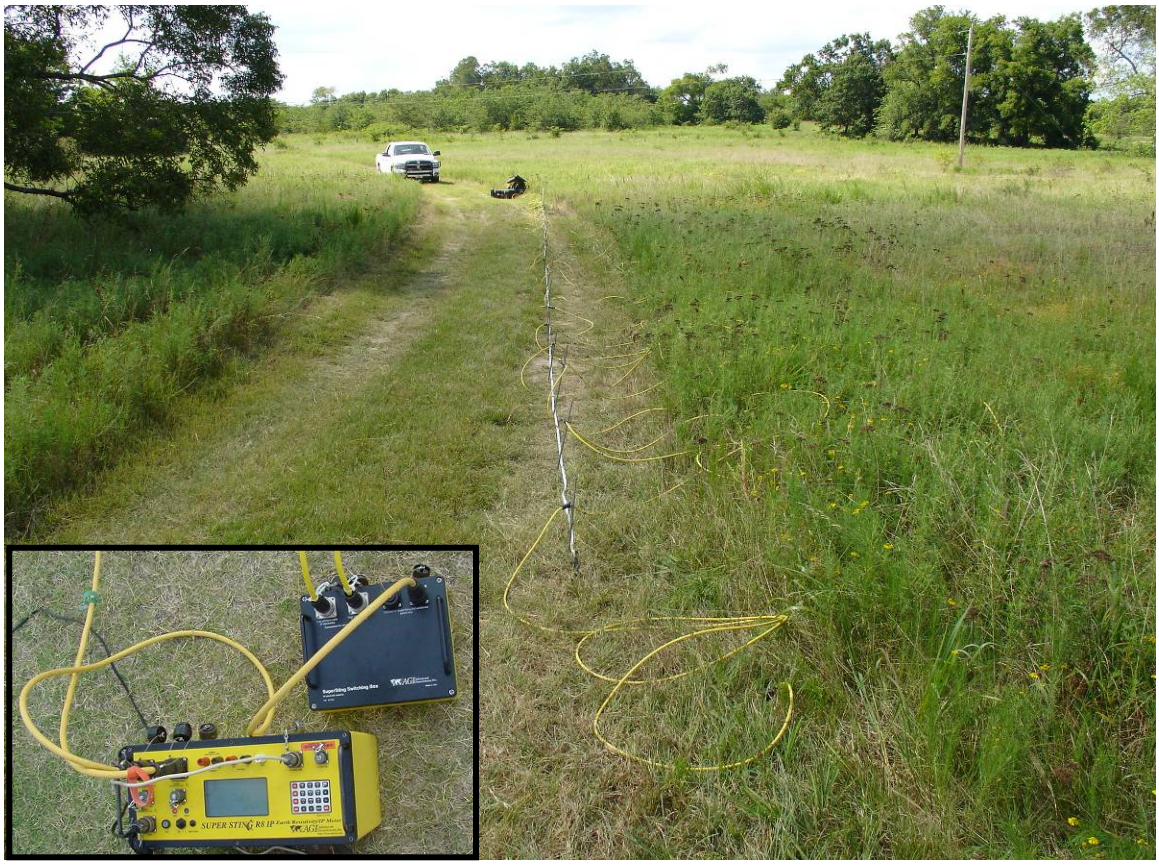

Figure 5: ERI surface electrodes and cables deployed to collect ERI Line AS1.25C1. Lower left: SuperSting R8 Earth Resistivity meter

The system consisted of 56 stainless steel electrodes (3/8-inch diameter) that were hammered in to the ground along a straight line at a specific spacing between electrodes. The total length of each of the lines varied from 68.75 meters to 495 meters (Figures 5, 6 and 7). Table 2 shows the ERI dataset information for both study sites.

The spacing used on each line was determined to provide the appropriate depth of imaging for the study area along with sufficient lateral distance to meet the project objectives. The depth of imaging at the site also varied from approximately 14 meters to 99 meters below the surface. The electrodes were connected via geophysical cables and the cables were connected to an AGI SuperSting resistivity meter and its components.

Site	Dataset	Electrode spacing (m)	Total Line Length (m)	~Depth of image (m)
Arbuckle Simpson Ranch	AS2.5A1	2.5	137.5	28
	AS1.25C1	1.25	68.75	14
	ASR5.00B	5	275	55
	ASRWE01A	5	275	55
	QTZSG01	9	495	99
Devil's Den	DEV0102	1.25	68.75	14
	DEV03	1.5	82.5	17

Table 2: ERI dataset information for both study sites.

Once each of the survey lines were laid out in the field, the resistivity instrument gathered a significant amount of data related to the electrical properties of the subsurface. Seven ERI datasets were collected during 2007- 2008. OSU collected ERI data using a proprietary high resolution ERI survey technique (developed by Oklahoma State University) known as the Halihan-Fenstemaker Technique (Halihan et al, 2005). The data was checked for quality and integrity in the field; full data reduction and processing were performed off-site.

Figure 6: ERI line locations and drilling targets at the Arbuckle-Simpson Ranch site

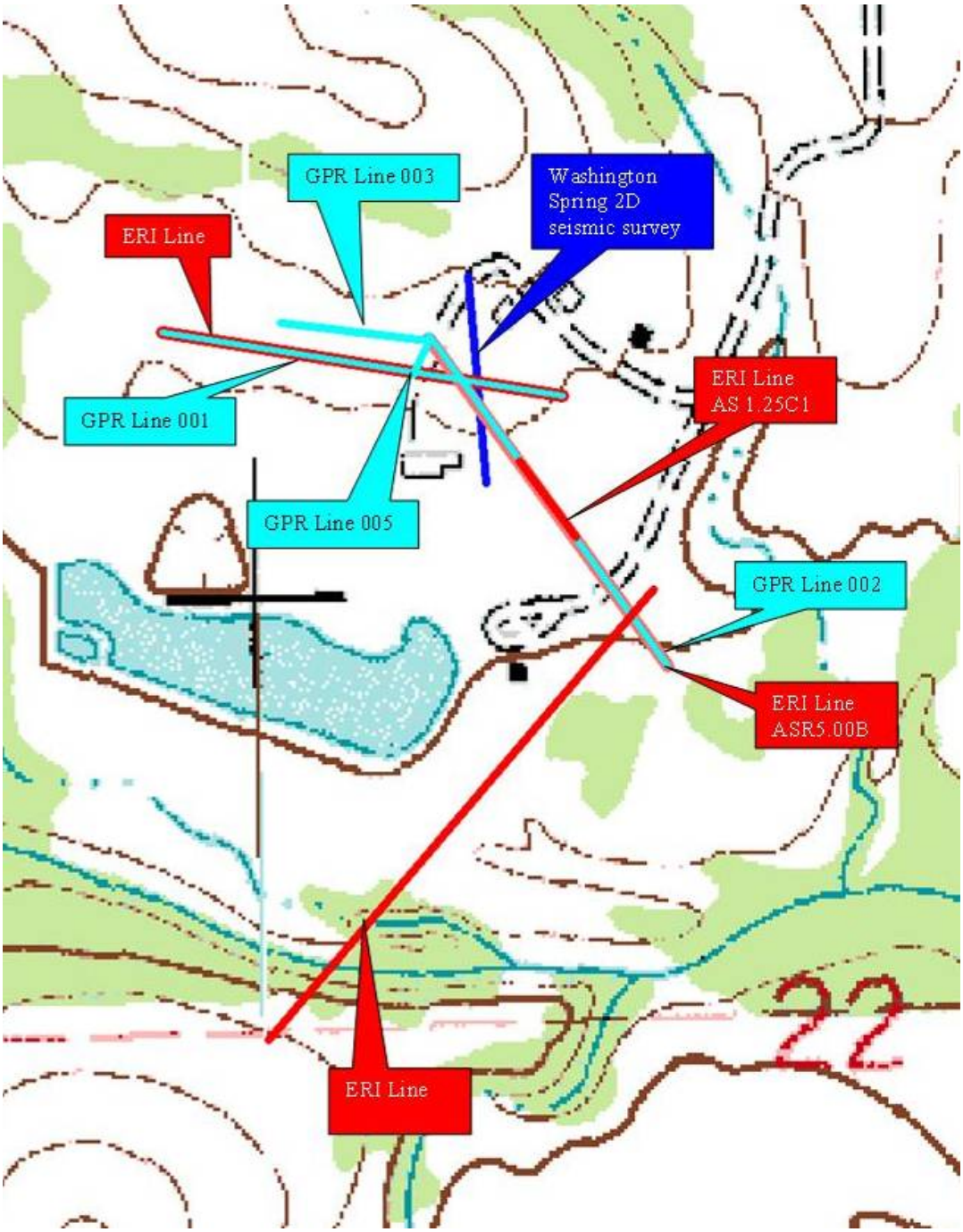

Figure 7: ERI and GPR locations at the Arbuckle-Simpson Ranch and Devil's Den sites.

4.2 ERI Data Reduction

Following field data collection, proprietary post-processing techniques were used to develop a final electrical resistivity image of the subsurface for each survey.

The raw data files collected in the field were post processed, including a more thorough review of data quality and integrity. Data points not meeting an established statistical

error criteria (i.e., typically less than 5 percent of the overall data set) are removed from the data set so that the resulting survey image is not skewed. A final image for each survey was developed which contains a model of the electrical resistivity of the subsurface in units of ohm-meters. Changes in topography along the survey were accounted for using information from a Topcon differential GPS system and a Topcon laser level system during this data processing work.

The final images were developed by contouring and plotting the resistivity data for each survey line using a consistent color scheme for the site to allow for evaluation of the results of all surveys on a comparative basis. For this study, the conductive (i.e., less resistive) areas of the subsurface are illustrated by the blue colors and the more resistive (i.e., less conductive) areas of the subsurface are illustrated by green and orange colors. The resistivity of the sites was so variable, that two color schemes were employed, one for each site.

As a part of overall data quality control process, the resistivity data for the entire site was compiled and then a normalized color scheme for the images was created. This allows consistency in the color scheme so a reviewer can correlate the results from one survey to the results from another survey performed on the same site during the same timeframe.

4.3 ERI Data Interpretation Process

The magnitude of subsurface resistivity values will vary from site to site based on a number of factors, and is related to geological composition and to the chemistry of the groundwater and other fluids trapped in the pore spaces within the soil matrix and the presence or absence of buried debris and structures. For a typical site, fine materials such as clay and silt are generally less resistive (i.e., more conductive) while coarse sand and gravel are generally more resistive (i.e., less conductive). Should the soil (clay or sand) be dry, it will appear more resistive when dry and less resistive when wet.

Should a distinct groundwater table exist in the area being surveyed, the groundwater interface is often not seen in the survey images because the resistivity of the ground water is often times similar to the resistivity of the soil matrix. Additionally the presence of contaminants within the pore matrix can overshadow (electrically) the presence of groundwater or degree of saturation. The presence of fractures in bedrock geology often appear as a vertically oriented anomaly and may be either conductive or resistive depending on what type of fluid (e.g., clean groundwater and/or unweathered/weathered contamination) is present within the fracture.

ERI survey results do not immediately identify the composition of anomalies which may be caused by variations in geology and/or moisture content (or other factors). Final data interpretation is greatly enhanced by calibrating or benchmarking the electrical resistivity images against existing site data and/or follow-up confirmation boring data. This process lends much greater understanding of the subsurface and the survey images. Ideally, confirmation work is performed as soon as possible following the survey work such that minimal time is allowed for subsurface changes in groundwater quality, etc. that may cause changed electrical conditions in the surveyed areas. For this project, the confirmation data collected previously from direct push borings will be used to evaluate the efficiency of the technique following review of the preliminary interpretations provided

in this report at the Arbuckle Simpson ranch. Since the bedrock is exposed at the Devil's Den site, the features in the bedrock were recorded to compare with the ERI data.

4.4 Electrical Resistivity Imaging Results

Seven transect lines of data were collected. The entire dataset was of good quality with resulting inversion RMS errors between 3 and 6.5%. Processing of Arbuckle Simpson Ranch data eliminated 10-20% of noisy data, which is quite reasonable for these types of data., At the Devil's Den site, only 6% of the data was eliminated in processing for the line that was collected directly on bedrock. For the site collected on soil, 30% of the data was lost due to the extremely high resistivity contrast between the soil and the bedrock.

The interpretations of the datasets are as follows:

ERI Line AS2.5A1: This dataset was collected at the Arbuckle-Simpson Ranch. The image indicates three electrical layers, a conductive (0-250 ohm-meters) soil zone that extends to a depth of approximately 3 to 4 meters on the image. Below the soil zone is the slightly more resistive epikarst zone that extends to a depth of approximately 4 to 9 meters. Underneath the epikarst is a more resistive layer (>850 ohm-meters) indicating more intact zones of bedrock with possible fracturing between the distances of 30-40 meters and 70-75 meters on the image. This image comprised what is believed to be the background lithologic properties at the site.

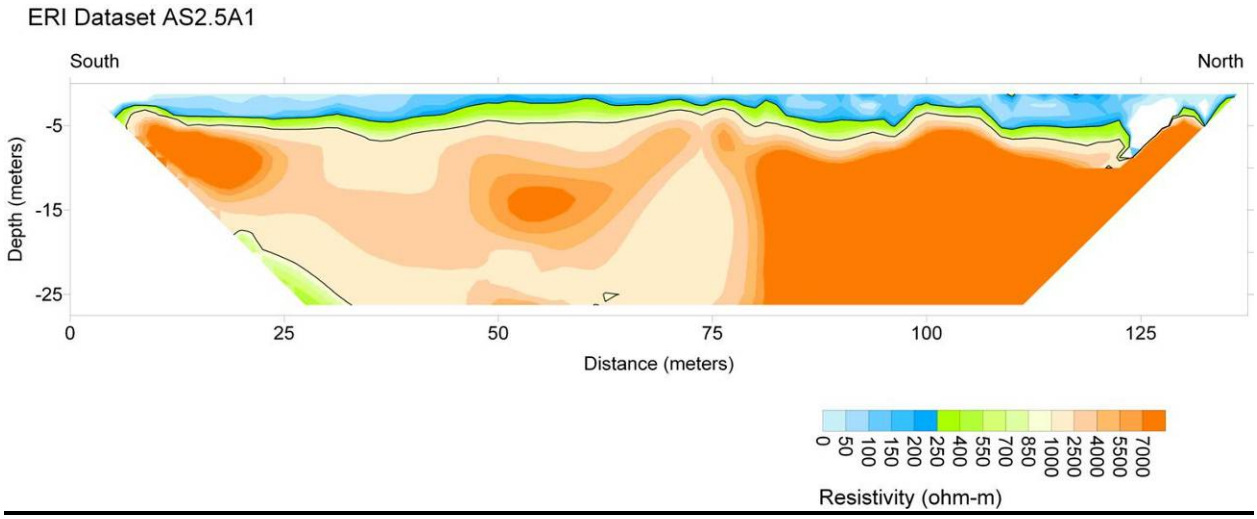

Figure 8: Image of ERI Line AS2.5A1

ERI Line AS1.25C1: This dataset was collected at the Arbuckle-Simpson Ranch. The image indicates two electrical layers, a soil zone less than 250 ohm-meters that extends down to an elevation of approximately 306 meters. This layer was evaluated with direct push cores and determined to be the extent of the soil layer (Sample, 2008). The next layer is more resistive (250-1000 ohm-meters) and extends downward to approximately 294 meters. The conductive area (0-250 ohm-meters) starting at the elevation 300m

going downward indicates an area of potentially increased weathering of the bedrock and a prospective pathway for fluids.

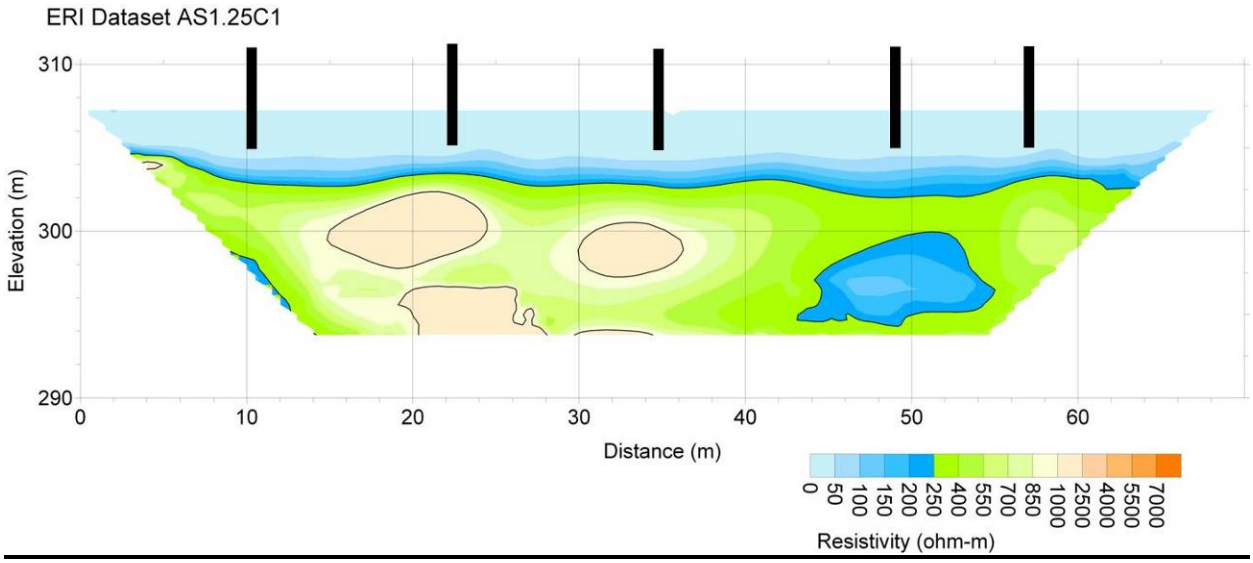

Figure 9: Image of ERI Line AS1.25C1

ERI Line ASR5.00B and ASRWE01A: These dataset were taken nearly orthogonal to each other on the Arbuckle-Simpson Ranch. Both images indicate three electrical layers, a conductive (0-250 ohm-meters) soil zone that extends to an elevation of approximately 300 meters on each image. At the 190 meter distance, both images indicates a fault zone extending vertically through the images. The resistivity values also indicate that an additional weathered zone exists for 100-150 meters away from the fault zone. This fault also corresponds to an inferred fault in the region.

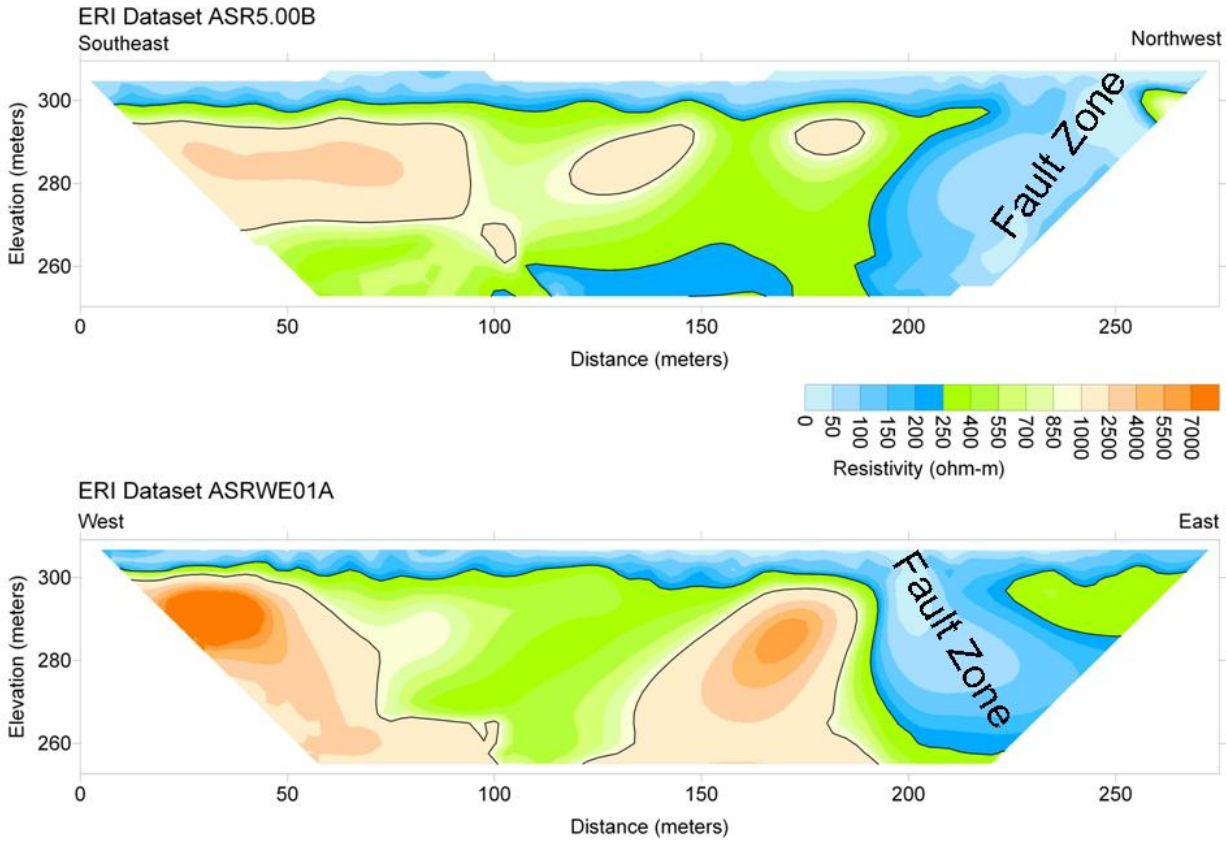

Figure 10: Images of ERI Line ASR5.00B and ASRWE01A

ERI Line QTZSG01: This dataset extends over the Blue River on the Arbuckle Simpson Ranch. This image indicates three electrical layers a conductive soil layer that extends down to 265-275 meters on the first 280 meters of the image. A more resistive layer of rock is found from 345-500 meters on the image and can be observed outcropping at the surface. Below 265 meters the image indicates variable resistivity in the data. Inferred flow paths for springs are indicated in the conductive areas (green and blue tones). The image suggests that the springs are not connected to the Blue River and that at this location, the Blue River is not well connected to the groundwater system.

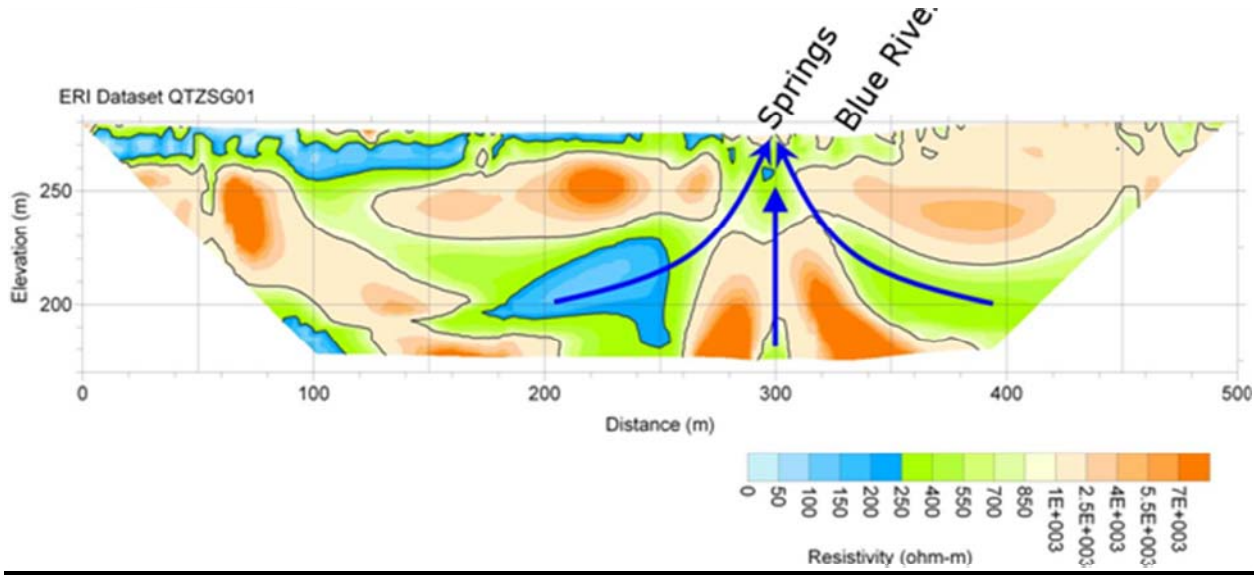

Figure 11: Image of ERI Line QTZSG01:

DEV0102: This data set was taken on exposed granite at the Devil's Den site. The resistivity scale was modified from the Arbuckle Simpson Ranch to accommodate extremely high resistivity values. This image indicates two electrical layers, a somewhat more resistive fractured layer extending down to an elevation of approximately 200 meters. Below the fractured layer is a more resistive less fractured layer extending down to an elevation of 189 meters. At the 40 meter and approximately 45 meter distance on the image granite dikes are indicated by elevated resistivity in the images. These dikes were also visible at the surface. The boundary between the layers may be a fracture zone caused by exposure of the granite.

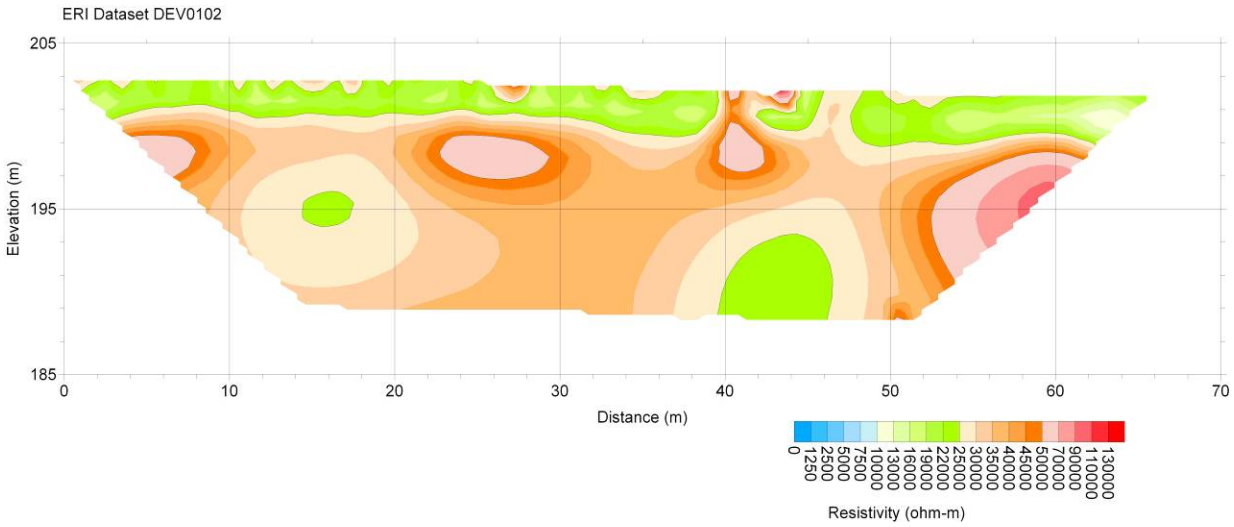

Figure 12: Image of DEV0102

DEV03: This dataset was taken over soil near the exposed granite at the Devil's Den site. This image indicates three electrical layers. For this dataset; a conductive and fractured zone (0-10000 ohm-meters) extends to an approximate elevation of 200 meters. Beneath the conductive zone is a more resistive zone (10,000-130,000 ohm-meters) indicating less fractured bedrock. The deeper conductive area may correspond to a fractured portion of the bedrock.

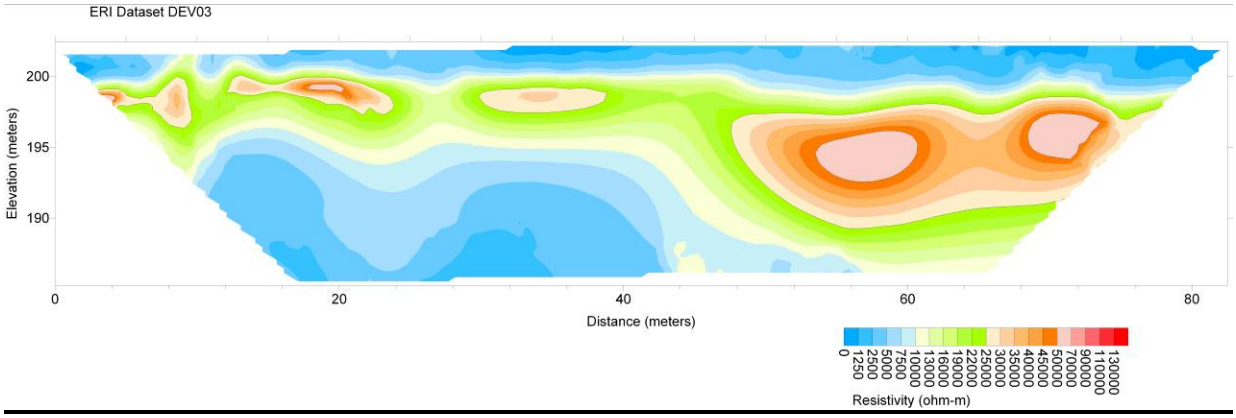

Figure 13: Image of DEV03

5.0 Geophysical and Geological Data Integration

5.1 A comparison of stratigraphic imaging by ERI and GPR methods

The focus of the present project is the correspondence of geological boundaries and vertical discontinuities as seen on the ERI resistivity inversion and on the GPR sections. The A-S Ranch has two coincident ERI and GPR surveys. Guided by the conceptual geological model at the site (Sample, 2008), we have compared the resistivity inversion and the reflection image for one of these pairs.

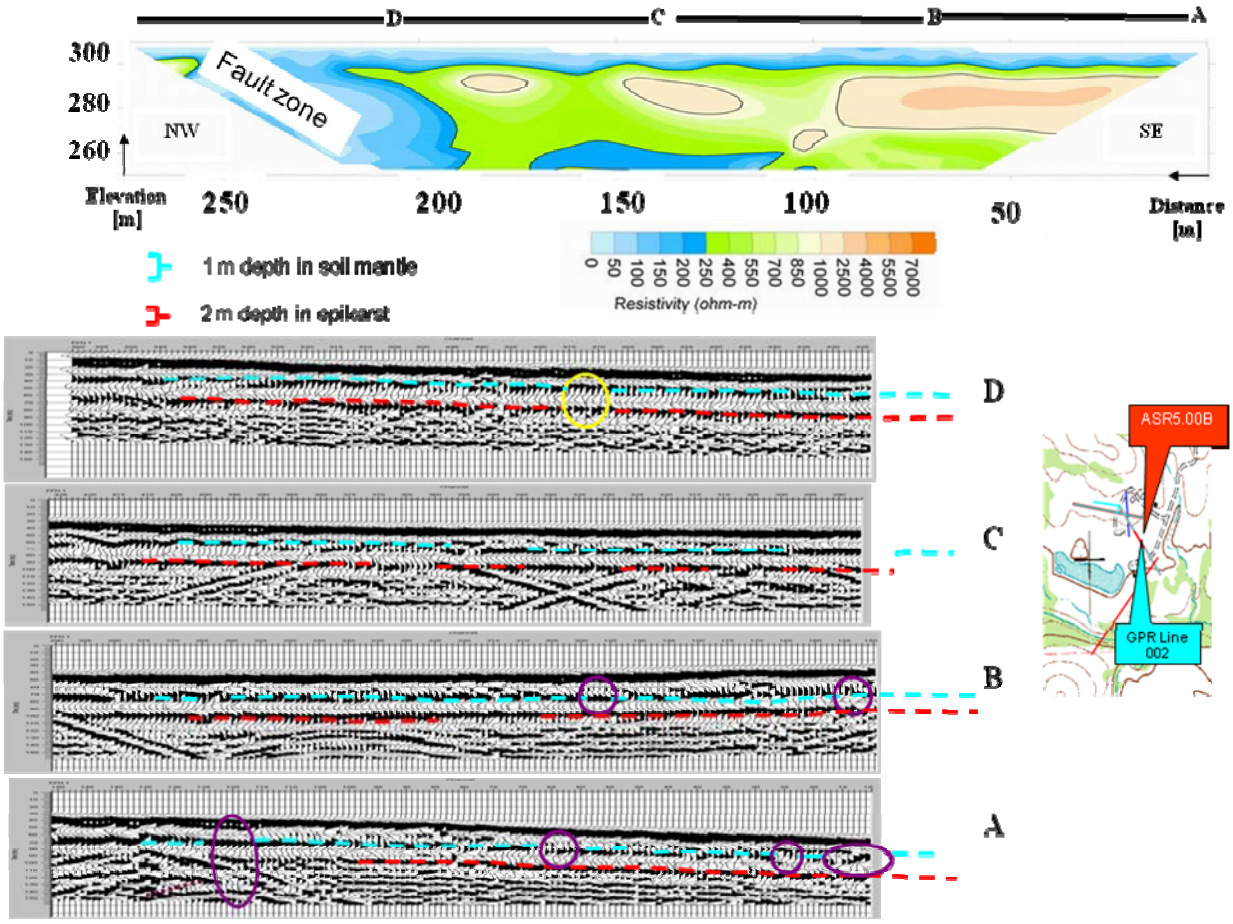

Figure 14: Comparison of ERI and GPR lines at the A-S Ranch. Upper (blue) and lower (red) boundaries are seen on both the ERI inversion (top) and the GPR reflection section (below).

A striking aspect of this comparison is that the two ERI resistivity boundaries—at 200 ohm-m and at the zone of rapid increase in resistivity from 200 to 2000 ohm-m—have a distinct appearance on the GPR line. The 5 m station spacing of the resistivity section does not see the lateral detail of the GPR reflections having a spacing of .5 m, but the blue dashed boundary occurs at a depth of approximately 2-3 m and the red dashed boundary approximately 2 m deeper on both lines.

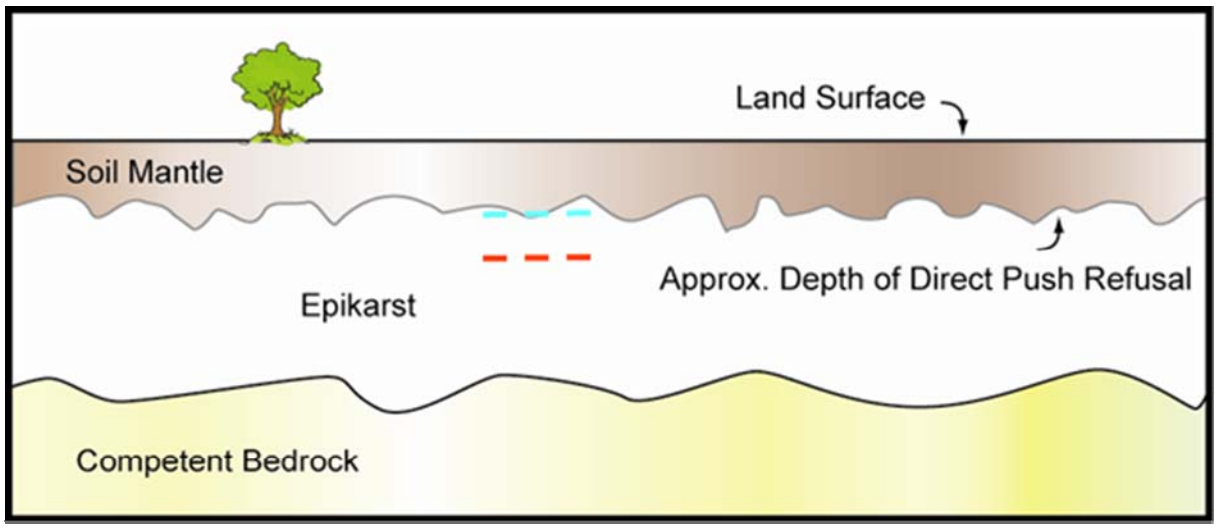

Figure 15: Conceptual model of the stratigraphy at the A-S Ranch (Sample, 2008). Base of the soil mantle (blue dashes) and a boundary within the epikarst (red dashes) are the same boundaries recognized on Figure 14.

Figure 15 indicates that the two geophysical boundaries correspond to the base of the soil mantle and to a boundary within the uppermost epikarst in the conceptual model. Geoprobe cores and logs (Sample, 2008) both indicate an abrupt change from soil to carbonate at a depth of approximately 2 m. (The location in the data is shown by the short red line in the Figure 14 inset.) This is also the depth at which the coring barrel was refused by a much more dense lithology (Sample, 2008). Because the ERI measurements are controlled by resistivity, GPR by permittivity, and core refusal by density one would expect somewhat different depths to these changes in physical properties. Water content would also effect the resistivity—and hence the ERI inversion— more than the permittivity and the GPR section.

Although both methods detect the presence of a fault beneath segment D, the broader delineation by the ERI inversion may be due to water saturation in the fault zone that has less effect on the GPR reflections.

5.2 A comparison of fracture detection by GPR methods and mapped fracture orientations

After processing all GPR lines at Devil's Den (Appendices A, B, and C), Kirchhoff 2D poststack time migration (Yilmaz, 2001) was applied to each line and the lines were combined into a 3D volume using the Kingdom Suite interpretation software (Davogustto and Young, in preparation). Finally, application of the maximum curvature attribute (Marfurt, 2006; Chopra and Marfurt, 2007) localizes the response of the fractures in the volume.

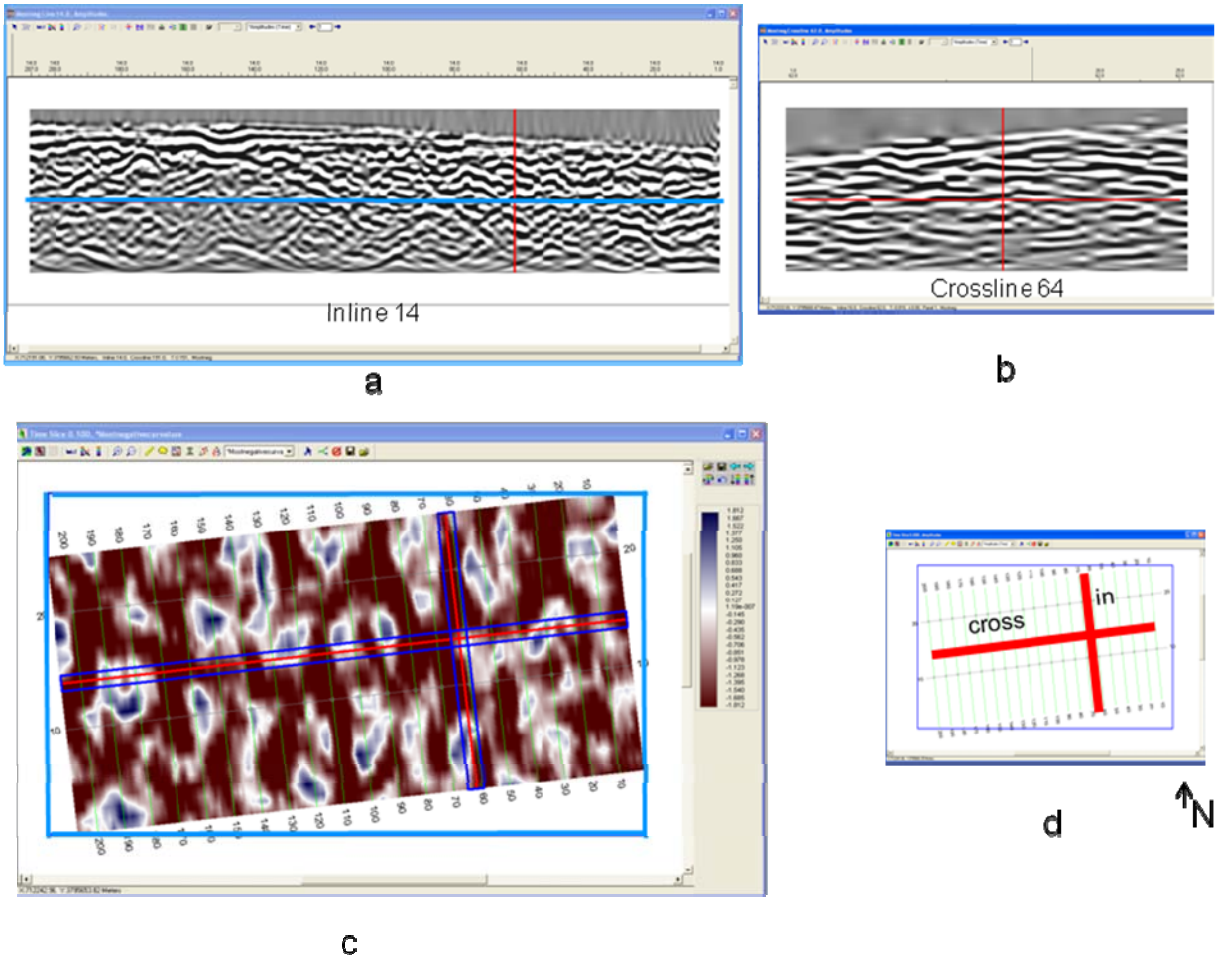

Figure 16: Three slices through the GPR volume . The inset (d) shows the locations of (a) inline 14 and (b) crossline 64 within the 3D survey. A time slice through the most negative curvature volume (c) at 100 ns (blue line on (a)) shows linear patterns not easily recognized on (a) and (b).

Figure 16a and b show two orthogonal lines (Figure 16d) from the GPR volume. A time slice through this volume (Figure 16c) shows linear patterns that we believe to be associated with the mapped fractures.

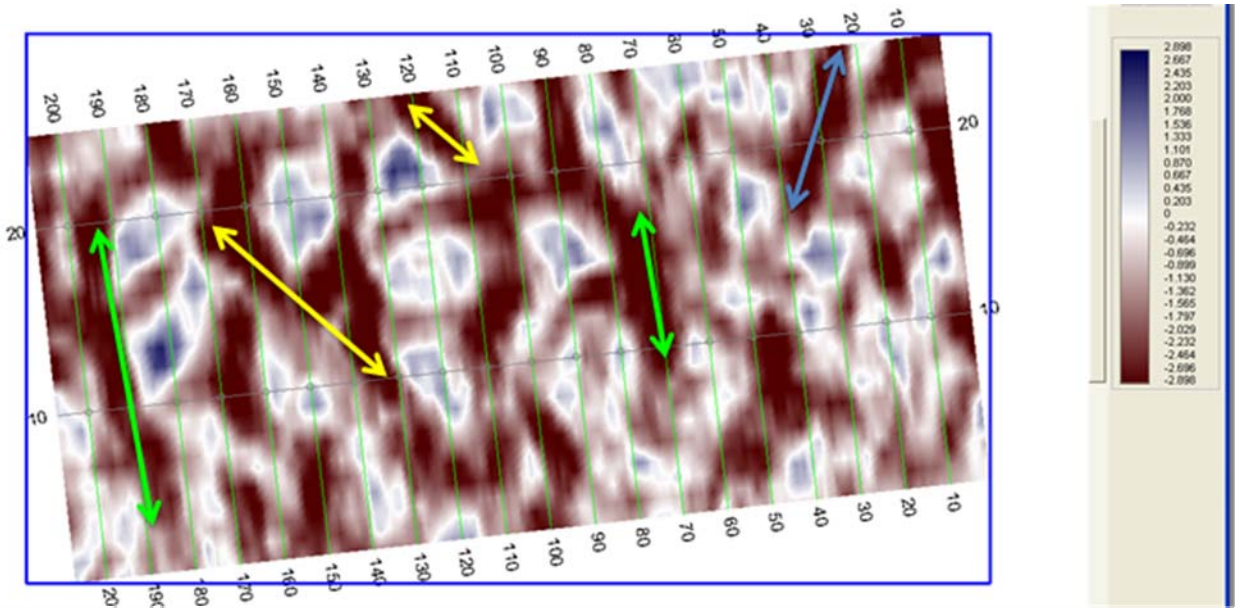

A)

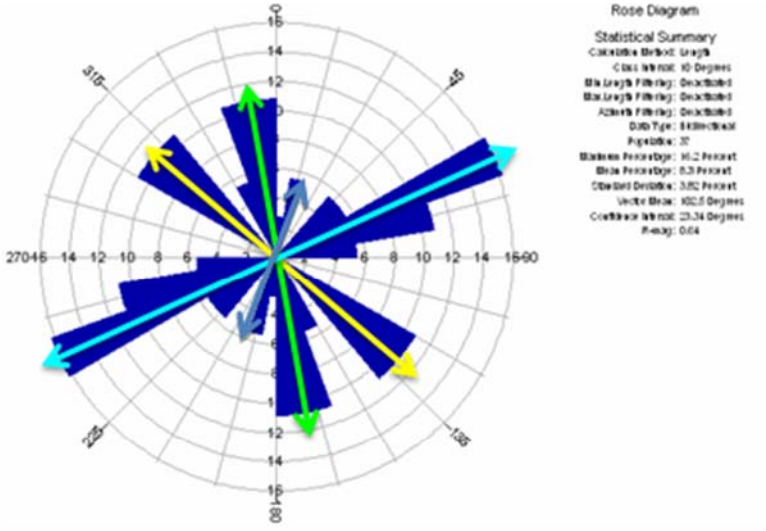

B)

Figure 17: (A) Time slice at 120 ns slice through the least curvature attribute volume. (B) Measured fracture directions are shown in the rose diagram. Principal strike directions of measured fracture sets are recognizable on the time slice as lineations of large negative curvature.

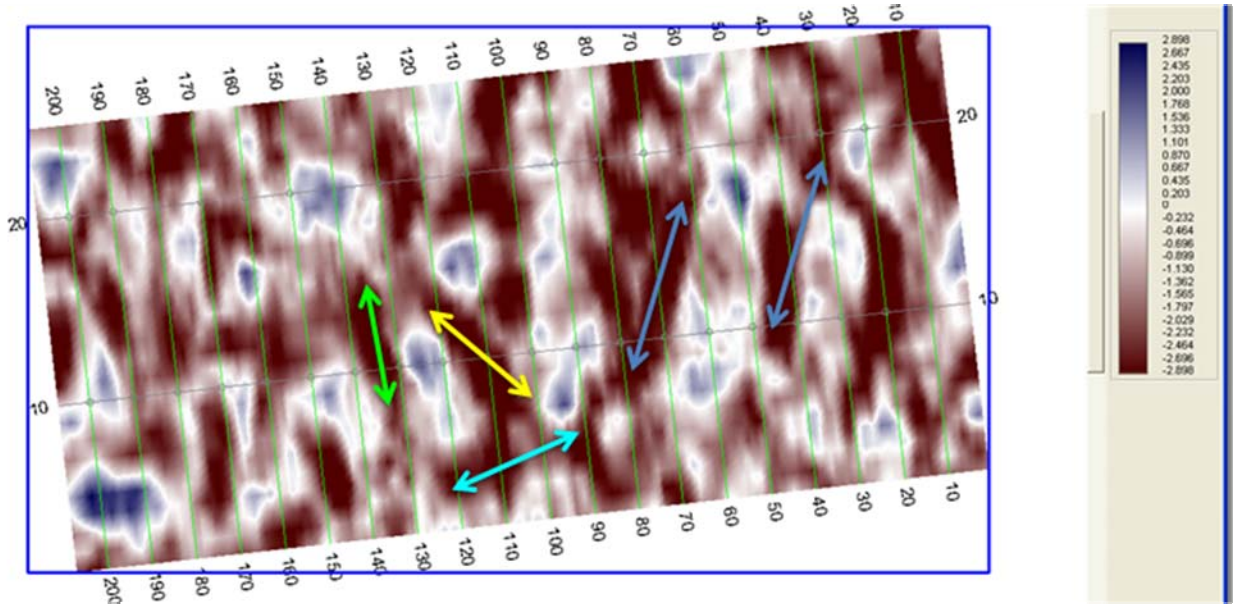

A)

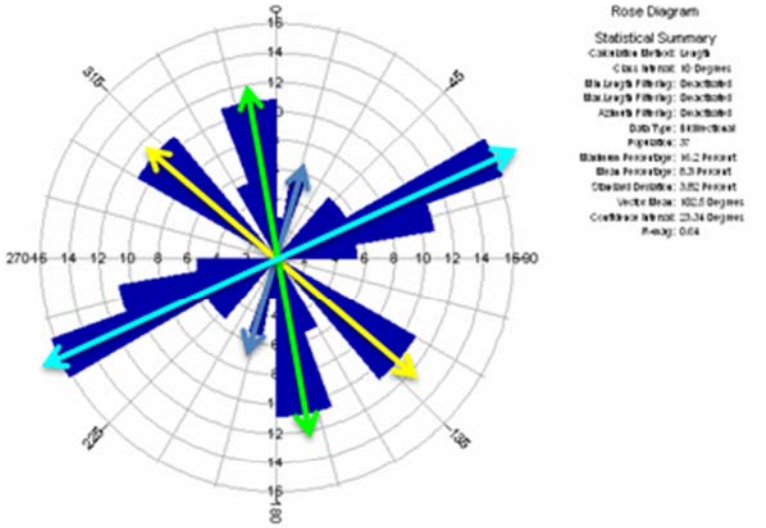

B)

Figure 18: (A) Time slice through least curvature attribute volume at 140 ns. (B) Measured fracture directions are shown in the rose diagram. Principal strike directions of fracture sets are recognizable on the time slice as lineations of large negative curvature.

The linear patterns appear even more clearly in time slices at other times than in Figure 16. Figure 17 and 18 are time slices at 120 and 140 ns, respectively, and for each the measured fracture directions in the rose diagram appear as high amplitude lineations on the time slices. All four directions in the rose diagram are represented in the lineations. Interestingly, the most populous fracture direction (blue in the rose diagram) is not represented in Figure 17A. Particular directions seem to be localized in different sectors

of the time slice, so a future task is to subdivide the fractures represented in the rose diagrams into outcrop locations where they were measured.

5.2 Uncertainties in conceptual models

Our operational model of fracture formation is that it is homogeneous over the surface of an outcrop area 50 m by 100 m. Given this assumption, a comparison of a rose diagram of fracture direction and intensity to patterns seen on time slices of GPR attribute volumes is sensible. However, expert opinion (David London, 2008, personal communication) suggests that preferred fracture packets exist over granite quarry floors elsewhere but that there is also variation in fracture intensity and in orientation over the quarry floor. In such a case, it would be important to break out the fracture information into location within the outcrop.

Perhaps the pattern variability suggested above is due to mining explosions used to quarry the granite and is of little relevance to fracture patterns on an unmined outcrop, such as at Devil's Den, where fractures are inherited from regional stress histories. In our examination of the GPR data at Devil's Den, though, we need to be guided by a clearer understanding of the fracturing process itself.

6.0 Conclusions

5.1 Relevance of combined ERI and GPR to fracture definition in the Arbuckle-Simspon Group

Collisional plate-tectonics affecting the interior of the North American craton caused faulting that disrupted the basement boundary (Ham et al., 1964). Reactivation of these basement faults in the Pennsylvanian and in younger tectonic episodes has resulted in the propagation of these faults upward through overlying formations. This fault reactivation is seen on exploration-scale seismic surveys in central Texas where the same sort of sub-vertical faults displace the basement and also overlying layers (Marfurt, 2006). Indeed, an exploration-scale 2D seismic survey acquired in 1980 by Anschutz across the eastern half of the Hunton Anticline in Oklahoma shows exactly the same sort of disruption by basement-penetrating faults. It also has the same fracture intensity (Kennedy and Young, in preparation). In both the Texas and Oklahoma cases equivalent rocks (the Ellenberger in Texas and the Arbuckle-Simpson in Oklahoma) are involved in the deformation, but in Oklahoma the deformed carbonate section is exposed at the surface. This offers a special opportunity to see if fracture patterns observed on the surface today can be linked to much earlier deformation at basement depths. This, in fact, is possible with the data from the present project. Data from the A-S Ranch comes from a stratigraphic position in the Arbuckle-Simpson Group that is 3000 ft above the base of the Group at its basement contact.

Encouragement that a link from the base of the Arbuckle-Simpson to a stratigraphic position 3000 ft higher is possible comes from an analysis of seismic data on the Hunton Anticline acquired at the A-S Ranch, the Spears Ranch, and the Anschutz 2D seismic line (Kennedy and Young, in preparation). These three locations represent shallow, intermediate, and deep seismic images, respectively, through this 3000 ft section of the Arbuckle-Simpson Group.

Further analysis of the fracture orientation in the present data and its relationship to fracturing extending from the surface to the basement leads to the exciting possibility that shallow geophysics could be a key to determining heretofore unmapped fracture locations in the Arbuckle-Simpson aquifer. Such information is valuable to definition of aquifer reservoir models constructed for flow simulations.

5.2 Enhancing initial success at geophysical imaging in carbonates and basement

The ERI method is a relatively new method that has just recently seen wide use in hydrologic surveys. The GPR method is somewhat more mature, but there is a paucity of published studies comparing results by both ERI and GPR methods over the same terrain.

The present 3D GPR survey on the Tishomingo granitic basement is the only such survey known to the authors. Others have investigated GPR imaging both on the ground surface and in boreholes for which logs are available in order to assess fracture density for the purpose of siting nuclear waste disposal chambers (Holloway et al., 1992). In

addition, underground surveys using GPR have been conducted in order to answer questions of roof stability in potash mining (Gendzwill, 1982).

Pioneering studies such as ours provide unusual new data and suggest new ways of answering important geological questions. However, seeing that ERI and GPR image stratigraphic or lithologic variation in the epikarst at the A-S Ranch, as we have done, is not equivalent to explaining the change in physical properties that is responsible for these observations. Converting the new observations to answers is a task that must build over time as the data is completely digested and geological patterns emerge from the geophysical representations.

Likewise, modern 3D GPR interpretation of fractures (eg., McClymont et al., 2008) takes its direction from innovations in the interpretation of 3-D seismic data using volume based attribute measurements (Marfurt, 2006). An early application of attribute analysis to 3D GPR data acquired over fractured fluvial sandstones (Young et al., 1997) revealed displacements in faulted horizons. The work at Devil's Den is more challenging as no layering exists and one must image diffractions from the fault itself. The work presented here is preliminary but points in a direction of further analysis (Davogustto and Young, in preparation).

7.0 References

Annan, A.P, 2005, Chapter 11: Ground penetrating radar, *in Near-surface geophysics,, Investigations in Geophysics, vol. 13, Society of Exploration Geophysicists [ed., Dwain K. Butler],357-438.*

Archie, G. E., 1942, The electrical resistivity log as an aid to determining some reservoir characteristics.: Transactions of the American Institute of Mechanical Engineers, v. 146, p. 389-409.

Chopra, S., Marfurt, K. (2007). Seismic curvature attributes for mapping faults/fractures, and other stratigraphic features: CSEG RECORDER, 32 (9), 37-41.

Daily, W., A. Ramirez, A. Binley, and D. LaBrecque, 2004, Electrical resistance tomography: The Leading Edge, p. 438-442.

Gendzwill, D. J., 1982, Induced earthquakes at a potash mine near Saskatoon, Canada, Canadian Journal of Earth Science, 19, 466-475.

Ham, W.H., Denison, R.E., and Merritt, C.A., 1964, Basement rocks and structural evolution of Southern Oklahoma, Oklahoma Geological Survey Bull. 95, 302 pp.

Herwanger, J. V., M. H. Worthington, R. Lubbe, and A. Binley, 2004, A comparison of cross-hole electrical and seismic data in fractured rock: Geophysical Prospecting, v. 52, p. 109-121.

Holloway, A.L., Stevens, K.M., Lodha, G.S., 1992, The results of surface and borehole radar profiling from permit area B o the Whiteshell Research Area, Manitoba, Canada, Fourth International Conference on Ground Penetrating Radar, Rovaniemi, Finland, conference proceedings [ed. Pauli Hanninen and Sini Autio], Geological Survey of Finalnd, Special Paper 16, 329-337.

Marfurt, K.J, (2006), Seismic attribute mapping of structure and stratigraphy, Distinguished Instructor Series, No. 9, Society of Exploration Geophysicists, 226 pp.

McClymont, A.F., Green, A.G., Streich, R., Horstmeyer, H., Tronicke, J., Nobes, D.C., Pettinga, J., Campbell, J., Langridge, R., 2008, Visualization of active faults using geometric attributes of 3D GPR data: An example from the Alpine Fault Zone, New Zealand, Geophysics, 73, 2, B11-B23.

Niwas, S., and O. A. L. de Lima, 2003, Aquifer parameter estimation from surface resistivity data: Ground Water, v. 41, p. 94-99.

Purvance, D. T., and R. Andricevic, 2000a, Geoelectric characterization of the hydraulic conductivity field and its spatial structure at variable scales: Water Resources Research, v. 36, p. 2915-2924.

Purvance, D. T., and R. Andricevic, 2000b, On the electrical-hydraulic conductivity correlation in aquifers: Water Resources Research, v. 36, p. 2905-2913.

Ramirez Meija, D., and Young, R.A., Fracture orientation in sedimentary rocks using multi-component ground-penetrating radar measurements, *The Leading Edge,* 26, 8, 1010-1017.

Ramirez, A., W. Daily, D. LaBrecque, E. Owen, and D. Chesnut, 1993, Monitoring an underground steam injection process using electrical resistance tomography, Water Resources Research, United States, American Geophysical Union: Washington, DC, United States, p. 73.

Sample, M.A., 2008, Characterization of the Epikarst over the Hunton Anticline, Arbuckle-Simpson Aquifer, Oklahoma, MS Thesis, School of Geology, Oklahoma State University,
, 220 pp.

Suneson, N. H., 1997, Pontotoc and Johnston Counties, Oklahoma. An Introduction and Field-Trip Guide:Prepared for the Annual Meeting of the Oklahoma Chapter of The Nature Conservancy.

Stollar, R. L., and P. Roux, 1975, Earth resistivity surveys; a method for defining ground-water contamination, Ground Water, United States, National Water Well Association, Ground-Water Technology Division : Urbana, IL, United States, p. 145.

Van Nostrand, R. G., and K. L. Cook, 1966, Interpretation of Resistivity Data, Geological Survey Professional Paper, United States Government Printing Office, Washington, United States Geological Survey.

Yilmaz, O (2001). *Seismic Data Analysis: Processing, Inversion and Interpretation of Seismic Data Volume I*, Tulsa: Society of Exploration Geophysicists.

Young, R.A., Sun, J., 1999, Revealing stratigraphy in ground-penetrating radar data using domain filtering, Geophysics, 64, 2, 435-442

Young, R.A., Deng, Z., Marfurt, K.J., and Nissen, S.E., 1997, 3-D dip filtering and coherence applied to GPR data: a study, The Leading Edge, 1011-1018.

Appendix A

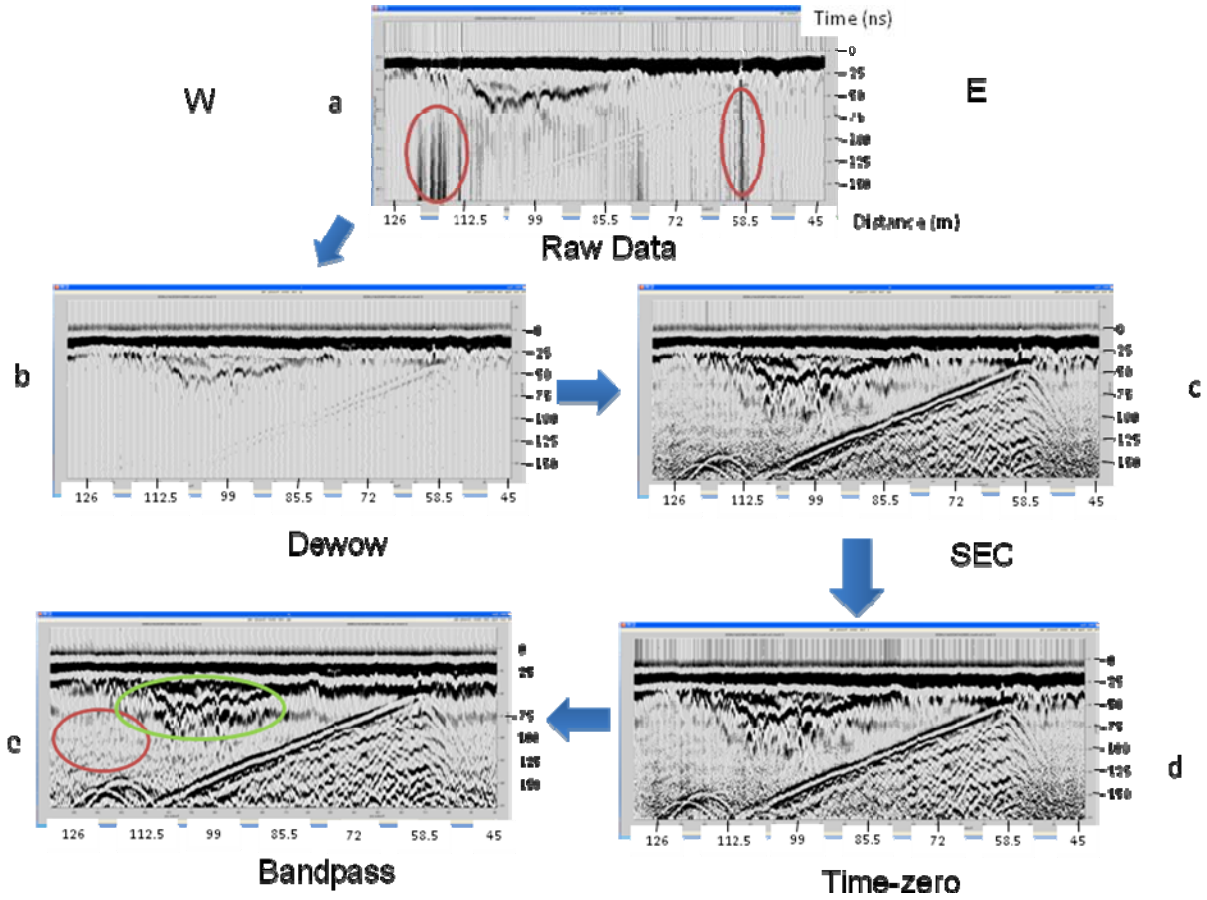

Figure A1: Processing steps for the Arbuckle-Simpson Ranch data. (a) A segment of raw data for GPR Line 2 between 45 and 126 m. (b) Data after dewow filter applied. The dewow filter is used to remove very low frequency components of the data associated with inductive phenomena or dynamic range limitations of the equipment (red ellipses in (a)). (c) Spherical and Exponential Compensation restores amplitude attenuation of the signal as it propagates through the ground. After the SEC is applied, features in the middle and deep part of the record are enhanced (green ellipses). Noise is also introduced (yellow arrows). (d) Time-zero correction aligns the airwave reflection starting time (yellow) on all traces. (e) Band pass filtering removes the background noise (yellow arrows in (d)) and high frequency noise revealed by the SEC gain (yellow arrows in (c)) thus giving a cleaner record (red ellipses).

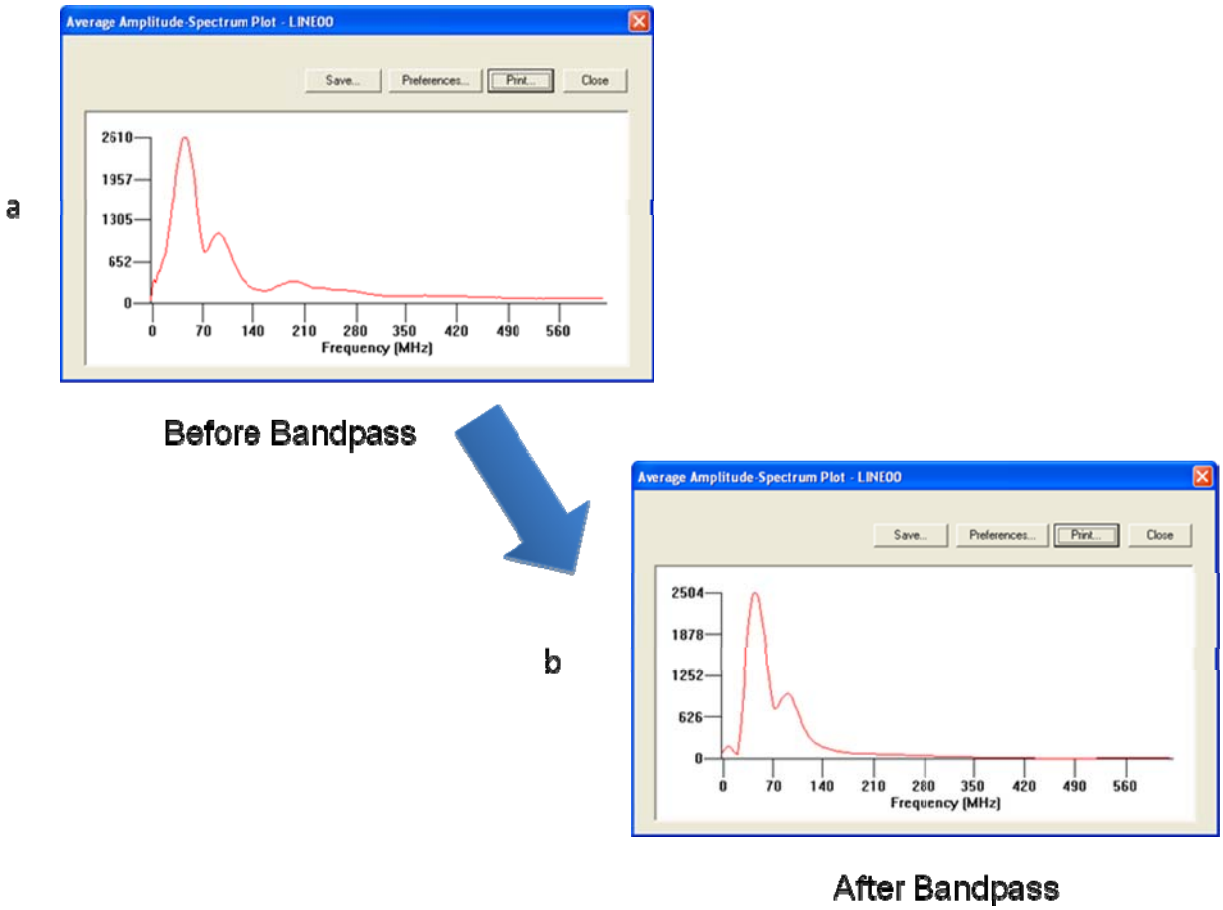

Figure A2: (a) Amplitude spectrum of the record before band pass filtering. Corner frequencies are 20 – 40 – 100 and 200 MHz. Notice the two imprints of noise: a low frequency slope (0 – 10 MHz) and a high frequency peak (150 - 280 MHz). The spectrum is broad with a maximum at about 60 MHz (b) Amplitude Spectrum after band pass filtering. Low frequency slope and high frequency peak are effectively suppressed. Spectrum has become more narrower—indicating a shorter reflection wavelet.

Appendix B

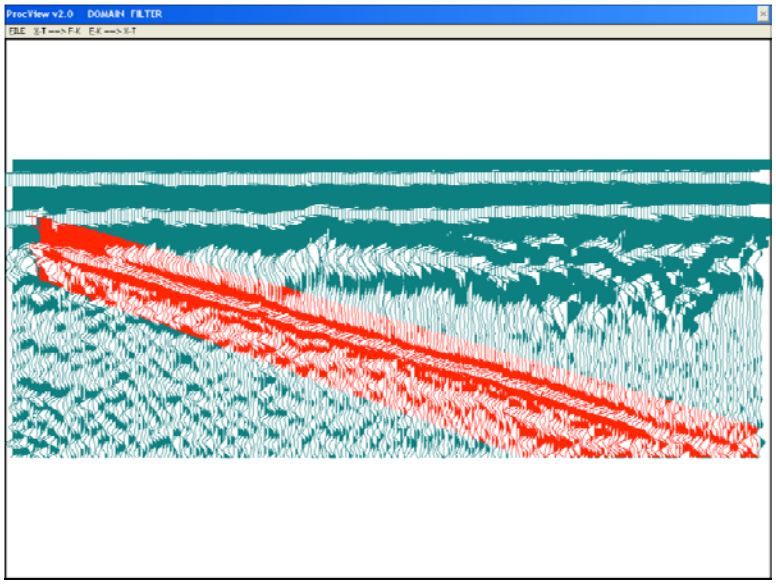

a)

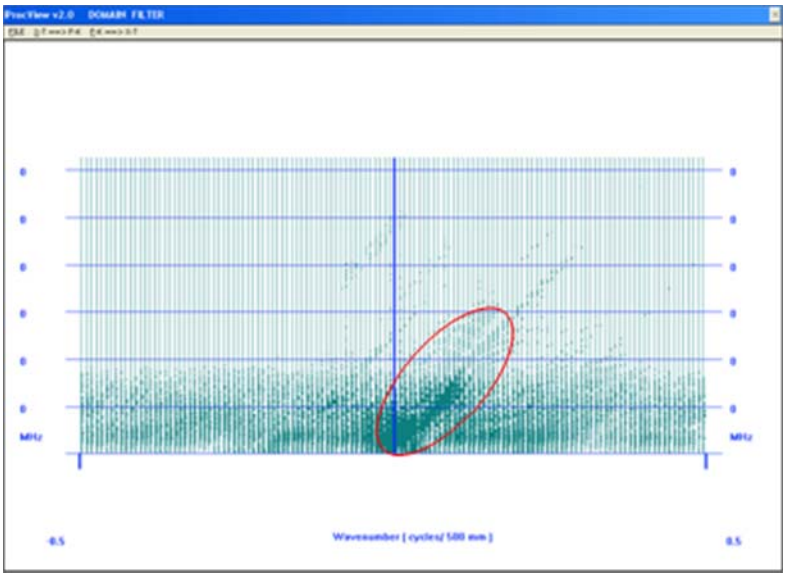

b)

Figure B1: The process of filtering by the Domain Filter. (a) Highlighted part of the record (red) is interpreted as noise. (b) The selected part of the record is displayed in the FK domain. Notice the high-amplitude dipping trend (red ellipse) that is the F-K equivalent of the red part highlighted in (a).

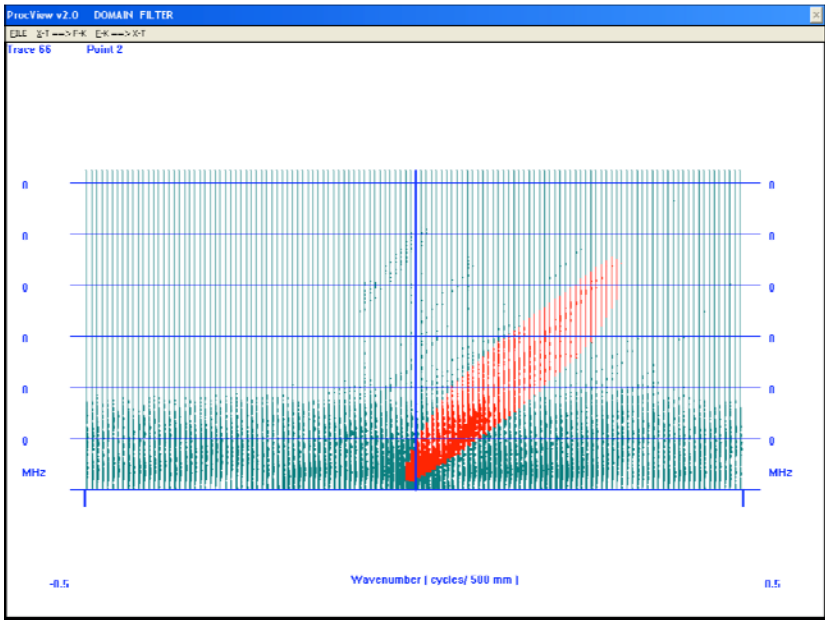

a)

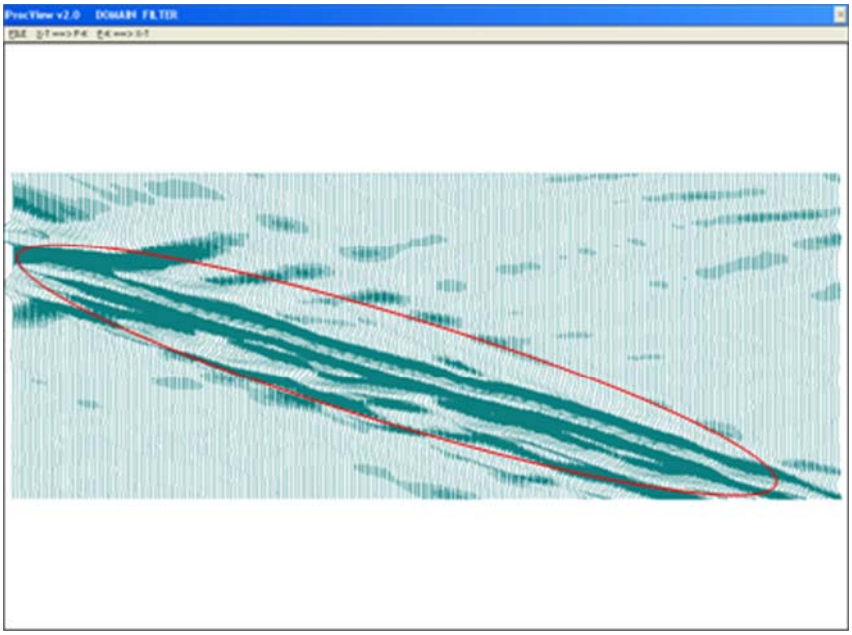

b)

Figure B2 (a) The selected part that is to be transformed back to the XT domain is highlighted in red. (b) After transformation, this is the part of the record (red ellipse) corresponding to the highlighted area that will be removed. Notice the FK transform artifacts outside the red ellipse.

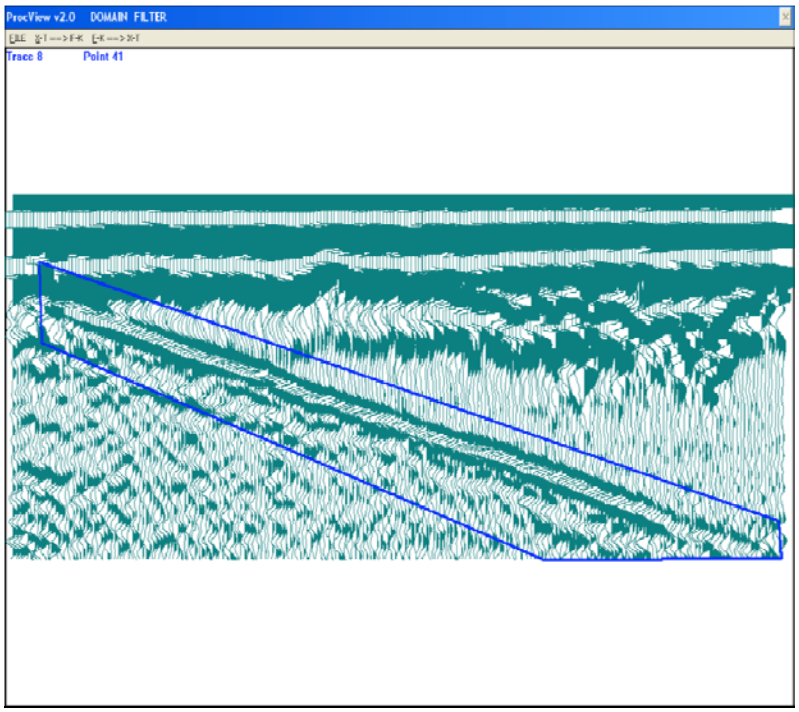

a)

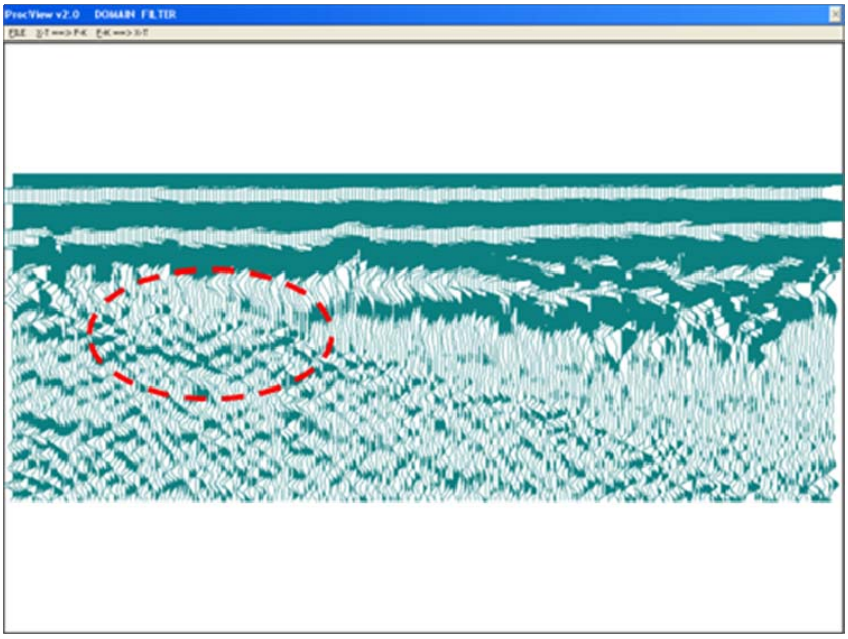

b)

Figure B3: (a) Record before the removal and (b) after the removal. Notice that the non-geological feature (blue rectangle) has been completely removed. The record has not been "damaged" by the artifacts introduced by the transforms when the filtering was performed. A stratigraphic sag (red dashed ellipse) is now apparent.

Appendix C

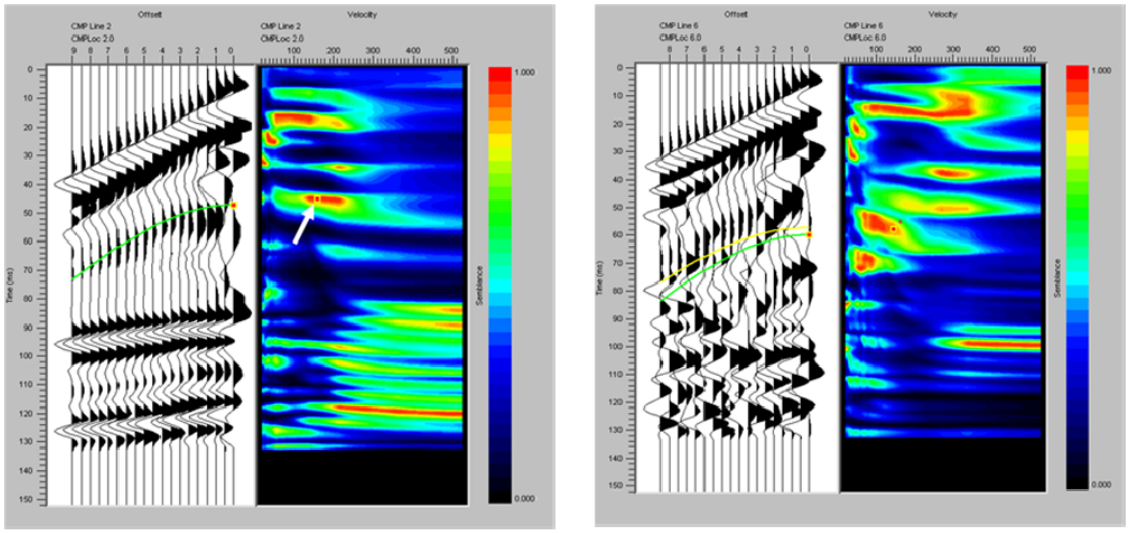

a b

Figure C1: (a) CMP 2---The red contour (right-hand side) of plot shows a large semblance value at 47 ns indicating an RMS velocity of .16 m/ns (white arrow). The corresponding reflection (left-hand side) fits the data well. (b) CMP 6---The RMS velocity indicated at 57 ns is .15 m/ns.

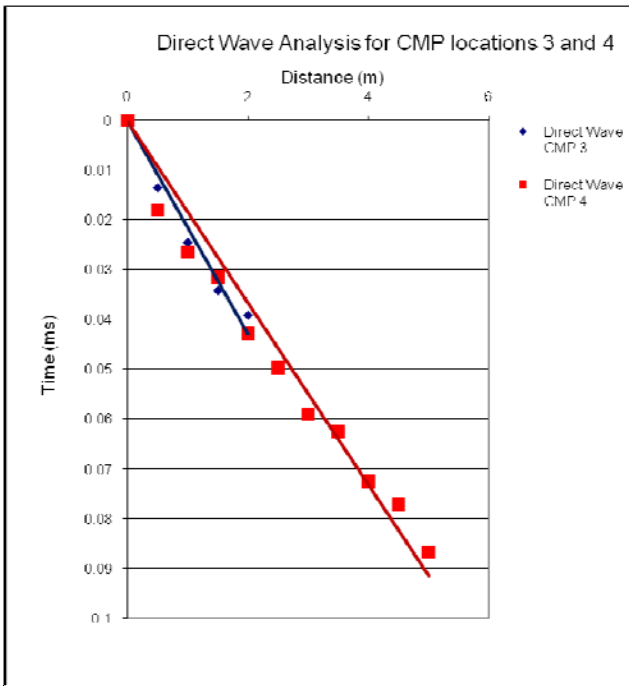

Figure C2: A least-squares fit to the travel times of the direct wave through the ground gives the velocity of the soil mantle.

Appendix D

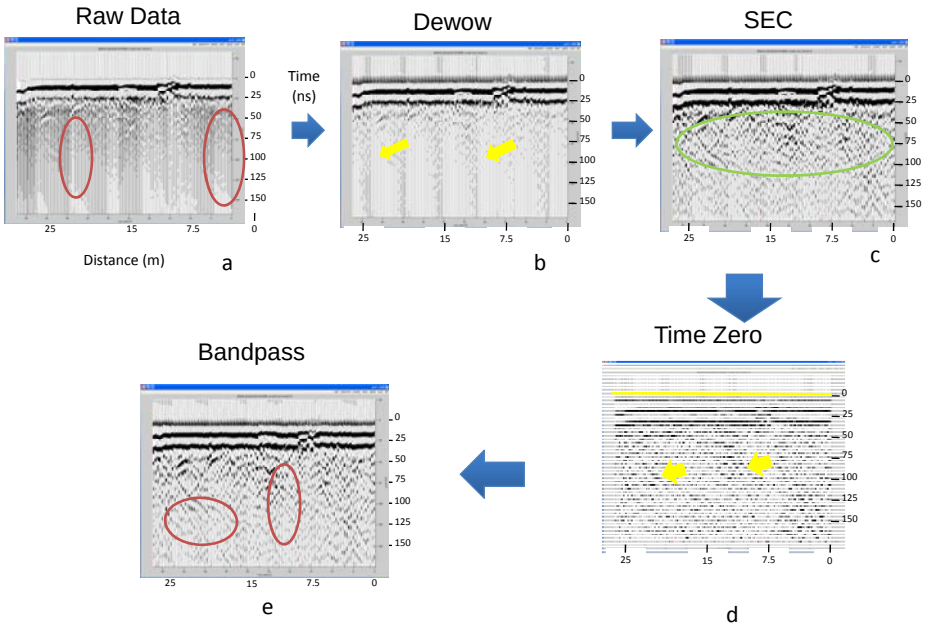

Figure D1: Processing steps for the Devils Den data. (a) Raw data. (b) Data after dewow filter applied. Dewow filter is used to remove very low frequency components of the data (red ellipses). Notice that there is still some low frequency component present (yellow arrows). (c) Spherical and Exponential Compensation restores amplitude attenuation of the signal as it propagates through the ground. After the SEC is applied, features in the middle and deep part of the record are enhanced (green ellipses). (d) Time-zero correction aligns the airwave reflection starting time (yellow) on all traces. (e) Band pass filtering removes the background noise (yellow arrows in (d)) and high frequency noise revealed by the SEC gain (yellow arrows in (c)) thus giving a cleaner record (red ellipses).

Appendix D

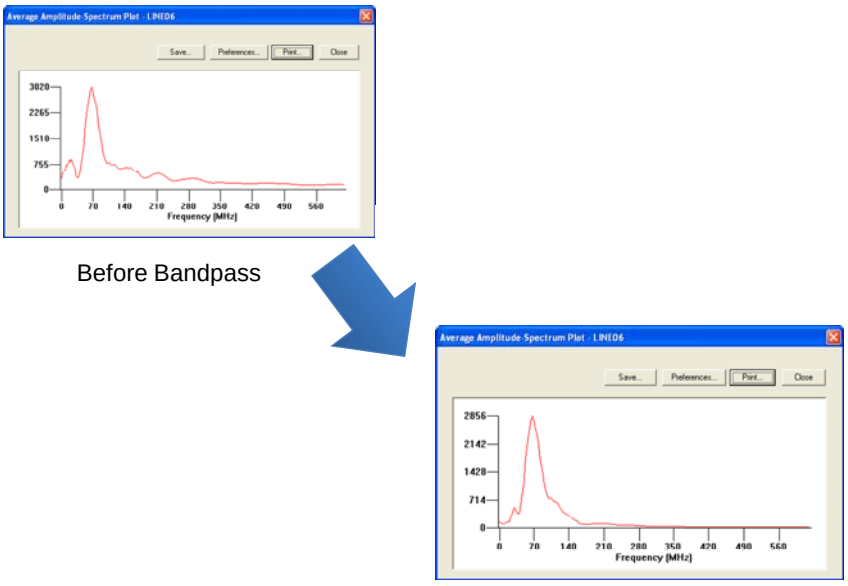

Figure D2: (a) Amplitude spectrum plot of the record before the band pass filter cut frequencies are 20 – 40 – 100 and 200 MHz. Notice the low frequency peaks (0 – 10 MHz) and the high frequency peak (150 - 350 MHz). The spectrum is broad with a maximum at about 70 MHz (b) Amplitude Spectrum after band pass filterinr. High frequency components are effectively suppressed as well as the low frequency components. The spectrum has become narrower with the maximum at about 70 MHz.

Appendix E

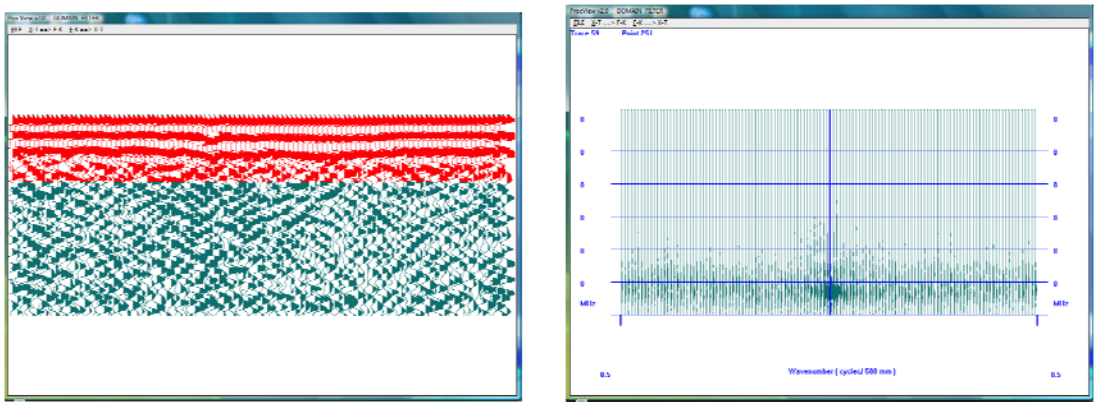

a b

Figure E1: (a) The highlighted part of the record (red) is interpreted as noise. This is the airwave direct arrival which is very strong in the shallow part of the record and might be masking some horizontal fractures or other features. (b) The selected part of the record is displayed in the FK domain.

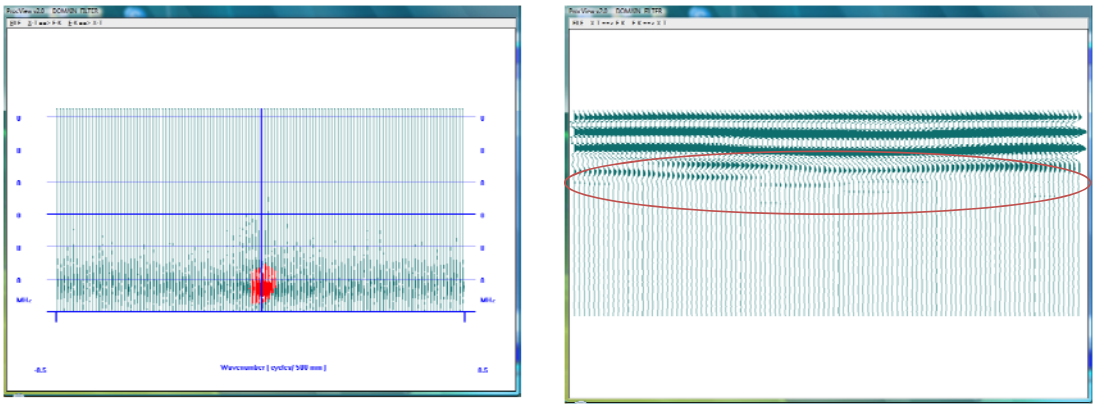

a b

Figure E2: (a) The selected part that is to be transformed back to the XT domain is highlighted in red. (b) After transformation the part of the record (red ellipse) corresponding to the highlighted area that will be removed. Notice the FK transform artifacts outside the red ellipse that are of minor relevance.

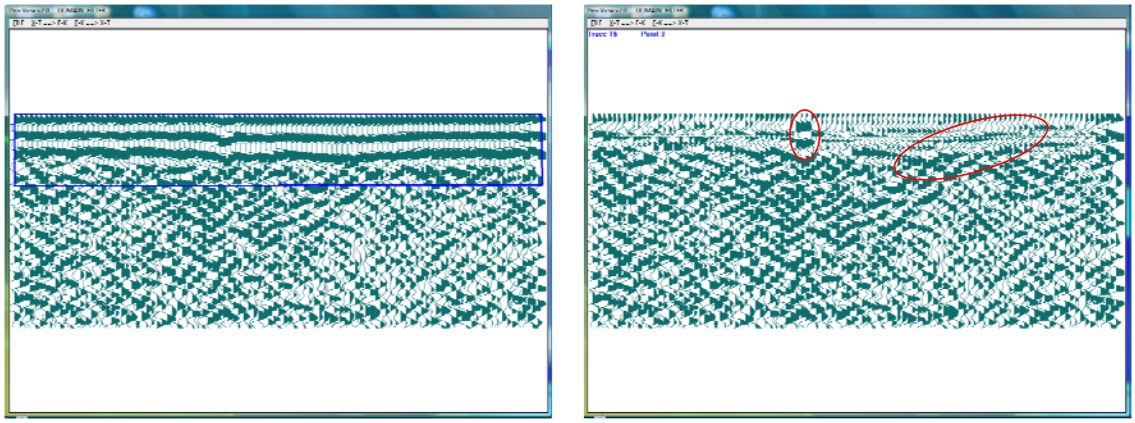

a b

Figure E3: Record before the removal (a) and after the removal (b) of the airwave. The airwave is gone and the record has not been “damaged” by artifacts introduced by the transforms. Shallow diffractions due to fractures at the surface of the outcrop have been revealed (red circles).

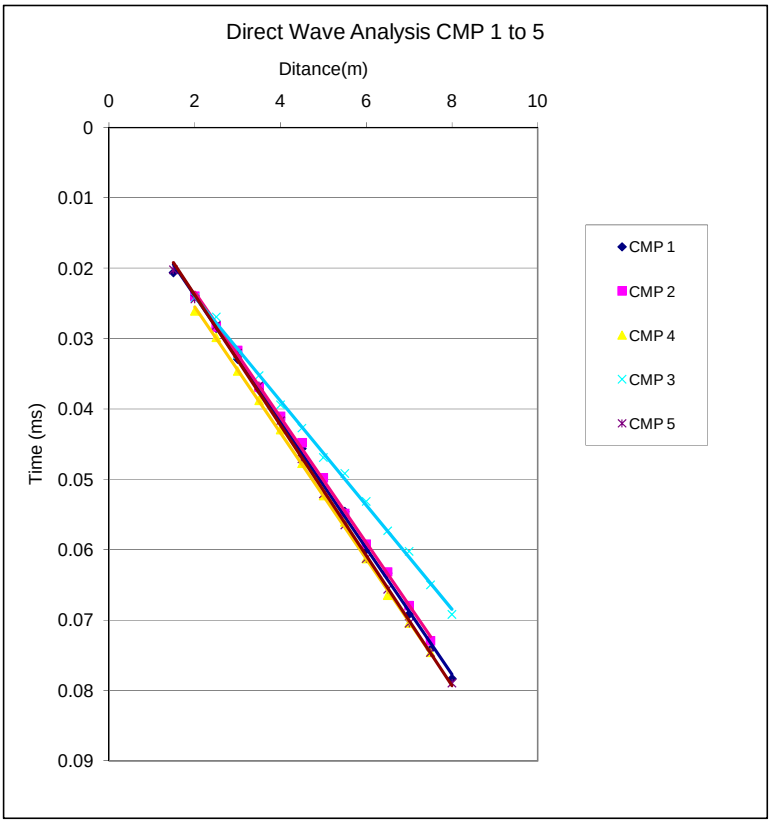

Velocity CMP 1 = 0.111 m/ns

Velocity CMP 2 = 0.112 m/ns

Velocity CMP 3 = 0.135 m/ns

Velocity CMP 4 = 0.112 m/ns

Velocity CMP 5 = 0.108 m/ns

Figure F1: Velocity of the Tishomingo granite at Devil's Den determined from the GPR direct arrival at 5 different locations on the outcrop.